



1 **Distribution of planktonic biogenic carbonate organisms in the Southern Ocean south of**
2 **Australia: a baseline for ocean acidification impact assessment**

3
4 Thomas W. Trull^{1,2,3}, Abraham Passmore^{1,2}, Diana M. Davies^{1,2}, Tim Smit⁴, Kate Berry^{1,2}, and Bronte
5 Tilbrook^{1,2}

6
7 1. Climate Science Centre, Oceans and Atmosphere, Commonwealth Scientific and Industrial
8 Research Organisation, Hobart, 7001, Australia

9 2. Antarctic Climate and Ecosystems Cooperative Research Centre, Hobart, 7001, Australia

10 3. Institute of Marine and Antarctic Studies, University of Tasmania, Hobart, 7001, Australia

11 4. Utrecht University, Utrecht, 3508, Holland

12
13 *Correspondence to:* Tom Trull (Tom.Trull@csiro.au)

14
15 **Abstract**

16 The Southern Ocean provides a vital service by absorbing about one sixth of humankind's annual
17 emissions of CO₂. This comes with a cost – an increase in ocean acidity that is expected to have
18 negative impacts on ocean ecosystems. The reduced ability of phytoplankton and zooplankton to
19 precipitate carbonate shells is a clearly identified risk. The impact depends on the significance of these
20 organisms in Southern Ocean ecosystems, but there is very little information on their abundance or
21 distribution. To quantify their presence, we used coulometric measurement of particulate inorganic
22 carbonate (PIC) on particles filtered from surface seawater into two size fractions: 50-1000 µm to
23 capture foraminifera (the most important biogenic carbonate forming zooplankton) and 1-50 µm to
24 capture coccolithophores (the most important biogenic carbonate forming phytoplankton). Ancillary
25 measurements of biogenic silica (BSi) and particulate organic carbon (POC) provided context, as
26 estimates of the abundance of diatoms (the most abundant phytoplankton in polar waters), and total
27 microbial biomass, respectively. Results for 9 transects from Australia to Antarctica in 2008-2015
28 showed low levels of PIC compared to northern hemisphere polar waters. Coccolithophores slightly
29 exceeded the biomass of diatoms in Subantarctic waters, but their abundance decreased more than 30-
30 fold poleward, while diatom abundances increased, so that on a molar basis PIC was only 1% of BSi
31 in Antarctic waters. This limited importance of coccolithophores in the Southern Ocean is further
32 emphasized in terms of their associated POC, representing less than 1 % of total POC in Antarctic
33 waters and less than 10% in Subantarctic waters. NASA satellite ocean colour based PIC estimates
34 were in reasonable agreement with (though somewhat higher than) the shipboard results in
35 Subantarctic waters, but greatly over-estimated PIC in Antarctic waters. Contrastingly, the NASA
36 Ocean Biogeochemical Model (NOBM) shows coccolithophores as overly restricted to Subtropical



37 and northern Subantarctic waters. The cause of the strong southward decrease in PIC abundance in
38 the Southern Ocean is not yet clear. Poleward decrease in pH is small and while calcite saturation
39 decreases strongly southward it remains well above saturation (>2). Nitrate and phosphate variations
40 would predict a poleward increase. Temperature and competition with diatoms for limiting iron
41 appear likely to be important. While the future trajectory of coccolithophore distributions remains
42 uncertain, their current low abundances suggest small impacts on overall Southern Ocean pelagic
43 ecology.



44 1. Introduction

45

46 Production of carbonate minerals by planktonic organisms is an important and complex part of the
47 global carbon cycle and climate system. On the one hand, carbonate precipitation raises the partial
48 pressure of CO₂ reducing the uptake of carbon dioxide from the atmosphere into the surface ocean;
49 on the other hand the high density and slow dissolution of these minerals promotes the sinking of
50 associated organic carbon more deeply into the ocean interior increasing sequestration [*P.W. Boyd*
51 *and Trull, 2007b; Buitenhuis et al., 2001; Klaas and Archer, 2002; Ridgwell et al., 2009; Salter et al.,*
52 *2014*]. Carbonate production is expected to be reduced by ocean acidification from the uptake of
53 anthropogenic CO₂, with potentially large consequences for the global carbon cycle and ocean
54 ecosystems [*Orr et al., 2005; Pörtner et al., 2005*].

55

56 The naturally low alkalinity of Southern Ocean waters makes this region particularly susceptible to
57 ocean acidification impacts, in that thresholds such as undersaturation of aragonite and calcite
58 carbonate minerals will be crossed sooner in this region than at lower latitudes [*Cao and Caldeira,*
59 *2008; McNeil and Matear, 2008; Shadwick et al., 2013*]. Important planktonic organisms include
60 coccolithophores (the dominant carbonate forming phytoplankton; e.g. [*Rost and Riebesell, 2004*]),
61 foraminifera (the dominant carbonate forming zooplankton; e.g. [*Moy et al., 2009; Schiebel, 2002*]),
62 and pteropods (a larger carbonate forming zooplankton, which can be an important component of fish
63 diets; e.g. [*Doubleday and Hopcroft, 2015; Roberts et al., 2014*]). The importance of carbonate
64 forming organisms relative to other taxa, which is poorly known in the Southern Ocean [*Watson W.*
65 *Gregg and Casey, 2007b; Holligan et al., 2010*], will influence the overall impact of ocean
66 acidification on ecosystem health. Satellite reflectance observations, mainly calibrated against
67 northern hemisphere PIC results, have been interpreted to suggest the presence of a “Great Calcite
68 Belt” in Subantarctic waters in the Southern Ocean, and also show high apparent PIC values in
69 Antarctic waters [*W M Balch et al., 2016; W M Balch et al., 2011*]. Our surveys were designed in part
70 to evaluate these assertions for waters south of Australia.

71

72 As a simple step towards quantifying the importance of planktonic biogenic carbonate forming
73 organisms in the Southern Ocean, we determined the concentrations of particulate inorganic carbonate
74 (PIC) for two size classes, representing coccolithophores (1-50 μm, referred to as PIC01) and
75 foraminifera (50-1000 μm, referred to as PIC50), from surface water samples collected on 9 transects
76 between Australia and Antarctica. We provide ecological context for these observations based on the
77 abundance of particulate organic carbon (POC) as a measure of total microbial biomass, and biogenic
78 silica (BSi), the other major phytoplankton biogenic mineral, as a measure of diatom biomass. This
79 provides a baseline assessment of the importance of calcifying plankton in the Southern Ocean south



80 of Australia, against which future levels can be compared. The baseline suggests lower PIC
81 abundances that suggested from the current satellite SPIC algorithms, especially in Antarctic waters.
82
83 In the discussion of our results, we interpret the BSi results as representative of diatoms, the PIC50 as
84 representative of foraminifera, and the PIC01 as representative of coccolithophores, including a
85 tendency to equate this with the distribution of the most cosmopolitan and best studied
86 coccolithophore, *Emiliana huxleyi*. These assumptions need considerable qualification. Most BSi is
87 generated by diatoms (~90%), with only minor contributions from radiolaria and choanoflagellates in
88 the upper ocean, making this approximation reasonably well supported [Hood *et al.*, 2006]. Similarly,
89 but less certainly, foraminifera are a major biogenic carbonate source in the 50-1000 μm size range,
90 but pteropods, ostracods, and other organisms are also important [Schiebel, 2002], so that this
91 approximation is weaker. We do not discuss the PIC50 results in any detail partly for this reason, but
92 more importantly because controls on foraminifera distributions appear to involve strongly differing
93 biogeography of several co-dominant taxa, rather than dominance by a single species [Be and
94 Tolderlund, 1971], and assessing these issues is beyond the scope of this paper. Attributing all the
95 PIC01 carbonate to coccolithophores relies on the assumption that fragments of larger organisms are
96 not important. This seems reasonable given that the larger PIC50 fraction generally contained 10-fold
97 lower PIC concentrations (as revealed in the Results section).

98
99 Our tendency to equate the PIC01 fraction with the abundance of *Emiliana huxleyi* is probably the
100 weakest approximation. It is not actually central to our conclusions, except to the extent that we
101 compare our PIC01 distributions to expectations based on models that use physiological results
102 mainly derived from experiments with this species. That said, this is a poor approximation in
103 Subtropical waters where the diversity of coccolithophores is large, but improves southward where
104 the diversity decreases (see Smith *et al.* 2017 for recent discussion), and many observations have
105 found that *Emiliana huxleyi* was strongly dominant in Subantarctic and Antarctic Southern Ocean
106 populations, generally >80% [Boeckel *et al.*, 2006; Eynaud *et al.*, 1999; Findlay and Giraudeau,
107 2000; Gravalosa *et al.*, 2008; Mohan *et al.*, 2008]. Of course, *Emiliana huxleyi* itself comes in
108 several strains even in the Southern Ocean, with differing physiology [Cubillos *et al.*, 2007; M. N.
109 Muller *et al.*, 2015; M.N. Muller *et al.*, 2017]. All these approximations are important to keep in mind
110 in any generalization of our results.

111

112 2. Methods

113 Sub-sections 2.1 and 2.2 present the sampling and analytical methods, respectively, used for the 8
114 transits across the Southern Ocean since 2012. Sub-section 2.3 details the different methods used
115 during the earlier single transit in 2008 and assesses the comparability of those results to the later
116 voyages. Sub-section 2.4 details measurements of water column dissolved nutrients, inorganic carbon



117 and alkalinity. Sub-section 2.5 provides details of satellite remote sensing data and the NASA Ocean
118 Biogeochemical Model used for comparison to the ship results.

119

120 **2.1. Voyages and sample collection procedures**

121 The locations of the voyages, divided into north and south legs, are shown in Figure 1. Voyage and
122 sample collection details are given in Table 1, where for ease of reference we have numbered the legs
123 in chronological order and refer to them hereafter as VL1, VL2, etc. Samples were collected from the
124 Australian icebreaker *RV Aurora Australia* for 4 voyages and from the French Antarctic resupply
125 vessel *l'Astrolabe* for 1 voyage. All samples were collected from the ships' clean seawater supplies
126 with intakes at ~4 m depth. Samples were collected primarily while underway, except during VL1
127 and VL3, which were operated as WOCE/CLIVAR hydrographic sections with full depth CTDs, with
128 samples collected on station.

129

130 For all voyages (except VL1, discussed in section 2.3 below), separate water volumes were collected
131 for the PIC, POC, and BSi analyses. The POC samples also yielded particulate nitrogen results -
132 referred to here as PON. The POC/PON and BSi samples were collected using a semi-automated
133 system that rapidly, ~ 1 minute, and precisely filled separate 1 L volumes for each analyte - thus these
134 samples are effectively point samples. In contrast, PIC samples were collected using the pressure of
135 the underway seawater supply to achieve filtration of large volumes (10's to 100's of litres) over ~2
136 hours. Thus these samples represent collections along ~20 miles of the ship track (except when done
137 at stations).

138

139 POC/PON samples were filtered through pre-combusted 13 mm diameter quartz filters (0.8 µm pore
140 size, Sartorius Cat#FT-3-1109-013) that had been pre-loaded in clean (flow-bench) conditions in the
141 laboratory into in-line polycarbonate filter holders (Sartorius #16514E). The filters were preserved by
142 drying in their filter holders at 60°C for 48 hours at sea, and returned to the laboratory in clean dry
143 boxes.

144

145 Biogenic silica samples were filtered through either 13 mm diameter nitrocellulose filters (0.8 µm
146 pore size, Millipore Cat#AAWP01300) or 13 mm diameter polycarbonate filters (0.8 µm pore size,
147 Whatman Cat#110409), pre-loaded in clean (flow-bench) conditions in the laboratory into in-line
148 polycarbonate filter holders (Sartorius #16514E). Filters were preserved by drying in their filter
149 holders at 60°C for 48 hours at sea, and returned to the laboratory in clean dry boxes.

150

151 PIC samples were collected by sequential filtration for two size fractions. After pre-filtration through
152 a 47 mm diameter 1000 µm nylon mesh and supply pressure reduction to 137 kPa, the ship clean
153 seawater was filtered through a 47 mm diameter in-line 50 µm nylon filter to collect foraminifera,



154 and then through a 47 mm diameter in-line 0.8 μm GF/F filter (Whatman Cat#1825-047) to collect
155 coccolithophores. The flow path was split using a pressure relief valve set to 55 kPa, so that large
156 volumes (~ 200 L) passed the 50 μm filter, and only a small fraction of this volume (~ 15 L) passed the
157 0.8 μm filter. Filtration time was typically 2 hours. Volume measurement was done by either metering
158 or accumulation. While still in their holders, the filters were rinsed twice with 3 mL of 20 mM
159 potassium tetraborate buffer solution (for the first couple of voyages and later deionized water) to
160 remove dissolved inorganic carbon, and blown dry with clean pressurised air (69 kPa). The filters
161 were then removed from their holders, folded, and inserted into Exetainer glass tubes (Labco Cat
162 #938W) and dried at 60 $^{\circ}\text{C}$ for 48 hours for return to the laboratory. In the following text, we refer to
163 the GF/F filter sample results (which sampled the 0.8 (~ 1) to 50 μm size fraction) as PIC01, and the
164 nylon mesh sample fraction (which sampled the 50-1000 μm size fraction) as PIC50.

165

166 2.2 Sample analyses

167 2.2.1 Particulate Organic Carbon and Nitrogen analysis

168 The returned filter holders were opened in a laminar flow bench and the filters cleanly transferred into
169 silver cups (Sercon Cat#SC0037), acidified with 50 μL of 2 N HCl and incubated at room temperature
170 for 30 minutes to remove carbonates, and dried in an oven at 60 $^{\circ}\text{C}$ for 48 hours. The silver cups were
171 then folded closed and the samples, along with process blanks (filters treated in the same way as
172 samples, but without any water flow onboard the ship) and casein standards (Elemental Microanalysis
173 OAS standard CatNo. B2155, Batch 114859) were sent to the University of Tasmania Central
174 Sciences Laboratory for CHN elemental analysis against sulphanilamide standards. Precision of these
175 analyses, based on standard variations was a few percent for POC and PON, but importantly the
176 processing blanks were larger and variable, and were corrected for separately for each voyage. For
177 VL2 and VL3, POC processing blanks averaged 25 ± 6 $\mu\text{g C}$ (1 sd, $n=2$) equating to 20% of average
178 sample values. For VL4 and VL5, POC process blanks averaged 14 ± 2 $\mu\text{g C}$ (1 sd, $n=4$) equating to
179 18% of average sample values. For VL6 and VL7, POC process blanks averaged 23 ± 3 $\mu\text{g C}$ (1 sd
180 $n=4$) equating to 28 % of average sample values.

181

182 2.2.2 Biogenic Silica analysis

183 Biogenic silica was dissolved by adding 4 mL of 0.2 M NaOH and incubating at 95 $^{\circ}\text{C}$ for 90 minutes,
184 similar to the method of [Paasche, 1973]. Samples were then rapidly cooled to 4 $^{\circ}\text{C}$ and neutralized
185 with 1 mL of 1 M HCl. Thereafter samples were centrifuged at 1880 g for 10 minutes and the
186 supernatant was transferred to a new tube and diluted with artificial seawater (36 g L^{-1} NaCl).
187 Biogenic silica concentrations were determined by spectrophotometry using an Alpkem model 3590
188 segmented flow analyser and following USGS Method I-2700-85 with these modifications:
189 ammonium molybdate solution contained 10 g L^{-1} $(\text{NH}_4)_6\text{Mo}_7\text{O}_{24}$, 800 μl of 10% sodium dodecyl



190 sulphate detergent replaced Levor IV solution, acetone was omitted from the ascorbic acid solution,
191 and artificial seawater was used as the carrier solution.

192

193 Biogenic silica standard concentrations were 0, 28, 56, 84, 112 and 140 μM . The sensitivity of
194 standard curves (forced through 0) varied by less than 1% (1 sd, n=5). The mean concentration of
195 repeated check standards (140 μM) run after every 12 samples was $140 \pm 0.5 \mu\text{M}$ (1 sd, n=64). The
196 average blank value was $0.014 \pm 0.003 \mu\text{moles per filter}$ (1 sd, n=9) for nitrocellulose filters and 0.010
197 $\pm 0.005 \mu\text{moles per filter}$ (1 sd, n=6) for polycarbonate filters, equating to ~2 % and 1.5 % of average
198 sample values, respectively.

199

200 **2.2.3 Particulate Inorganic Carbon analysis**

201 Particulate inorganic carbon samples were analysed by coulometry using a UIC CM5015 coulometer
202 connected to a Gilson 232 autosampler. The samples were analysed directly in their collection tubes,
203 by purging for 5 minutes with nitrogen gas, acidification with 1.6 mL (PIC50 - 50 μm nylon filters) or
204 2.4 mL (PIC01 - GF/F filters) of 1 N phosphoric acid, and equilibration overnight at 40°C. Samples
205 were analysed the following day with a sample analysis time of 8 minutes and a dried carrier gas flow
206 rate of 160 mL min^{-1} . Calcium carbonate standards (Sigma Cat#398101-100G) were either weighed
207 onto GF/F filters or weighed into tin cups (Sercon Cat# SC1190) and then inserted into Exetainer
208 tubes (some with blank nylon filters). Typical standard weights were circa 0, 50, 200, 1500 and 6500
209 μg . Standard curves for GF/F filters (forced through 0) across all voyages varied by less than 0.9% (1
210 sd, n=9), and for nylon filters by less than 0.6% (1 sd, n=10). The mean percentage recovery of
211 repeated check standards for GF/F filters was $100.5 \pm 3.9 \%$ (1 sd, n=29), and for nylon mesh filters
212 $100.2 \pm 1.9 \%$ (1 sd n=30). The average GF/F filter blank value was $0.67 \pm 0.26 \mu\text{g C}$ (1 sd, n=15)
213 equating to 2% of average sample values, and for nylon filters was $0.56 \pm 0.19 \mu\text{g C}$ (1 sd, n=21)
214 equating to 0.9% of average sample values.

215

216 **2.3 Distinct sample collection and analytical methods used during V1**

217 **2.3.1 Distinct sample collection procedures for VL1**

218 For VL1, single samples were collected at each location by both sequential filtration and
219 centrifugation of the underway supply over 1-3 hours. Despite the long collection times these
220 samples are effectively point samples because they were collected on station.

221

222 Sequential filtration was done using in-line 47 mm filter holders (Sartorius, Inc.) holding 3 sizes of
223 nylon mesh (1000 μm , 200 μm , 50 μm) followed by a glass fibre filter (Whatman GF/F, 0.8 μm
224 nominal pore size, muffled before use). These size fractions were intended to collect foraminifera (50-
225 200 μm) and coccolithophores (0.8-55 μm), and pteropods (200-1000 μm), but the largest size
226 fraction had insufficient material for analysis. The flow rate at the start of filtration was $25\text{-}30 \text{ L hour}^{-1}$



227 and typically dropped during filtration. The 0.8 μm filter was replaced if flow rates dropped below 10
228 L hour⁻¹. Sampling typically took 3 hours. Quantities of filtered seawater were measured using a flow
229 meter (Magnaught MIRSP-2RL) with a precision of +/-1%. After filtration, remaining seawater in the
230 system was removed using a vacuum pump. Filters were transferred to 75 mm Petri dishes inside a
231 flow bench, placed in an oven (SEM Pty Ltd, vented convection) for 3-6 hours to dry at 60 °C and
232 stored in dark, cool boxes for return to the laboratory.

233

234 A continuous flow Foerst type centrifuge [Kimball Jr and Ferguson Wood, 1964], operating at 18700
235 rpm, was used to concentrate phytoplankton from the underway system at a flow rate of 60 L per
236 hour, measured using a water meter with a precision of +/-1% (Arad). Sampling typically took 1-3
237 hours. After centrifugation, 500 mL of de-ionized water was run through the centrifuge to flush away
238 remaining seawater and associated dissolved inorganic carbon. This was followed by 50 mL of
239 ethanol to flush away the de-ionized water, ensure organic matter detached from the cup wall, and
240 speed subsequent drying. Inside a laminar flow clean bench, the slurry in the centrifuge head was
241 transferred into a 10 mL polypropylene centrifuge tube (Labserve) and the material on the wall of the
242 cup was transferred using 3 mL of ethanol and a rubber policeman. The sample was then centrifuged
243 for 15 minutes and 3200 rpm, and the supernatant (~7 mL) removed and discarded. The vial was
244 placed in the oven to dry for 12 hours at 60 °C and returned to the laboratory.

245

246 2.3.2 Distinct analytical procedures for VL1 samples

247 POC/PON analyses for the 0.8 μm size fraction collected by filtration were done by packing five 5
248 mm diameter aliquots (punches) of the 47 mm diameter GF/F filters into acid-resistant 5x8 mm silver
249 cups (Sercon SC0037), treating these with two 20 μl aliquots of 2 N HCl to remove carbonates [P
250 King *et al.*, 1998], and drying at 60 °C for at least 48 hours. For the 50 μm mesh filtration samples,
251 and the centrifuge samples, 0.5-1.0 mg aliquots of the dried (72 hours at 60 °C) centrifuge pellet
252 remaining after PIC coulometry were encapsulated in 4x6 mm silver cups (Sercon SC0036).

253 Analyses of all these sample types was by catalytic combustion using a Thermo-Finnigan Flash 1112
254 elemental analyzer calibrated against sulphanilamide standards (Central Sciences Laboratory,
255 University of Tasmania). Precision of the analysis was +/- 1 %. A blank correction for of 0.19 ± 0.09
256 $\mu\text{g C}$ was applied which represented 1.6 % of an average sample.

257

258 PIC concentrations were determined for subsamples of the 0.8 μm GF/F filters (half of the filter), the
259 whole 50 μm mesh screens, and the whole centrifuge samples by closed system acidification with HCl
260 and coulometry using a CM5011 CO₂ coulometer. The samples were placed in glass vials (or in the
261 case of the centrifuge tubes connected via an adaptor), connected to an acidification unit maintained at
262 60°C, acidified with an excess of 2 N HCl, and swept with a nitrogen gas-flow (~100 mL min⁻¹) via a
263 drier into the coulometry cell Calibration versus calcium carbonate samples provided precision of \pm



264 0.3%. However, for the 0.8 μm filter, precision was limited to 10 % by sub-sampling of the filter due
265 to uneven distribution. Blank corrections were applied to the 0.8 μm size fraction, being 2.4 ± 1.8 ug
266 C representing 8.8 % of an average sample. The 55 μm fraction blank correction was 3.3 ± 0.1 ug C,
267 representing 22 % of an average sample. Centrifuge pellet coulometry blank subtraction was 2.0 ± 0.1
268 ug C which was 2.8 % of an average sample.

269

270 Biogenic silica analysis of the residues remaining after PIC analysis of the centrifugation samples,
271 was by vortex mixing, an alkaline digest (0.2 N NaOH) in a 95°C water bath for 45 minutes, similar to
272 the method described by Paasche (1973). The samples were then cooled in an ice bath, 1 mL of 1 N
273 HCl added and mixed, and spun in a bench centrifuge for approximately 10 minutes to remove
274 undigested solids. 4 mL of each sample was transferred from the centrifuge tubes and filtered using a
275 syringe filter into a nutrient tube. Six mL of artificial seawater was added to make the sample up to 10
276 mL. Samples were then analysed using an Alpkem segmented flow analyzer [Eriksen, 1997].

277

278 **2.3.3 Comparison of VL1 to other voyages**

279 The first survey on VL1 in 2008 differed from later efforts in two important ways: i) POC and PIC
280 samples were collected by both filtration and centrifugation, ii) separate BSi samples were not
281 collected - instead BSi analyses were carried out only on the sample residues from PIC coulometric
282 sample digestions of the centrifuge samples. Comparison of POC and PIC results from the
283 centrifugation samples (effectively total samples without size fractionation) and the filtration samples
284 (separated into the PIC01 0.8-50 μm and PIC50 50-1000 μm size fractions) shows (Figure 2) that
285 filtration collected somewhat more PIC (order 20-30 %) and considerably more POC (order 200-300
286 %) than centrifugation. This fits with the possibility of loss of material from the continuous
287 centrifuge cup, with greater loss of lower density organic matter (and possible additional loss of
288 organic matter via dissolution in the ethanol rinsing step). Thus for comparison of VL1 POC and PIC
289 to the other voyages we use only the filtration results, thereby avoiding methodological biases. For
290 BSi, we do not have this possibility. Based on the low centrifuge yields for PIC and POC we can
291 expect that the VL1 BSi values are also too low. This is confirmed by comparison to the other
292 voyages which reveals that VL1 BSi values were lower than those of other voyages, especially in the
293 far south where BSi values were generally highest (data shown below), but nonetheless had similar
294 north-south latitudinal trends. For this reason, our further interpretation of the VL1 BSi results is only
295 in terms of these latitudinal trends.

296

297 **2.4 Analysis of nutrients, DIC, alkalinity, and calculation of pH and calcite saturation**

298 Nutrients were analysed onboard ship for VL1 to VL5, and on frozen samples returned to land for
299 VL6-9, all by the CSIRO hydrochemistry group following WOCE/CLIVAR standard procedures,



300 with minor variations [Eriksen, 1997], to achieve precisions of ~1% for nitrate, phosphate, and silicate
301 concentrations. Dissolved inorganic carbon (DIC) and alkalinity samples were collected in gas tight
302 bottles poisoned with mercuric chloride and measured at CSIRO by coulometry and open cell
303 titration, respectively [Dickson *et al.*, 2007]. Comparison to certified reference materials suggests
304 accuracy and precision for both DIC and alkalinity of better than $\pm 2 \mu\text{mol kg}^{-1}$. Full details were
305 recently published [Roden *et al.*, 2016]. Calculation of pH (free scale) and calcite saturation were
306 based on the Seacarb version 3.1.2 software (<https://CRAN.R-project.org/package=seacarb>), which
307 uses the default selection of equilibrium constants given in [Van Heuven *et al.*, 2011].

308

309 **2.5 Satellite derived ocean properties and the NASA Ocean Biogeochemistry Model**

310 The locations of oceanographic fronts in the Australian sector were estimated from satellite altimetry,
311 following the approach of [S. Sokolov and Rintoul, 2002], updated as follows. Absolute sea surface
312 height (SSH) was calculated by adding the sea surface height anomaly from AVISO+ [Pujol *et al.*,
313 2016] to the 2500 dbar reference level mean dynamic topography of [Olbers *et al.*, 1992]. The
314 positions of the fronts were then identified using the sea surface height contours corresponding to the
315 positions of the Southern Ocean fronts identified by [S. Sokolov and Rintoul, 2007a] in the region
316 100-180 °E. From this analysis, we show 8 fronts from north to south consisting of:

317 Fronts 1-3) north, middle, and south branches of the SAF, which bound the highest velocity jets of the
318 ACC.

319 Fronts 4-6) north, middle, and south branches of the Polar Front, associated with subsurface
320 temperature features related to the strength of the ACC and with the shoaling of CDW in the
321 overturning circulation.

322 Fronts 7-8) north and south branches of the Southern ACC front, marking weaker flows in Antarctic
323 waters of the ACC and occurring near where upwelling of old nutrient rich and relatively acidic
324 Circumpolar Deep Water comes closest to the surface.

325

326 We do not show the Subtropical Front that marks the northern boundary of the Southern Ocean, or the
327 Southern Boundary Front, which marks the southern edge of the ACC (separating it from westerly
328 flow in Antarctic shelf waters). This is because both features have weak, discontinuous SSH
329 signatures south of Australia: mesoscale eddies rather than the STF dominate the weak SSH field in
330 the SAZ, and detection of the Southern Boundary Front is confounded by proximity to the Antarctic
331 shelf where altimetry is impacted by other processes, including sea-ice cover for much of the year [S.
332 Sokolov and Rintoul, 2007a].

333

334 We considered using these dynamic heights and front locations as ordinates for the spatial
335 distributions of POC, PIC and BSi. In the core of the ACC (50-60 °S), this did help explain some
336 departures from monotonic north-south trends as resulting as resulting from meanders of the fronts,



337 but latitude was more strongly correlated with PIC abundance in the SAZ and with BSi in southern
338 ACC waters and Antarctic shelf waters, where dynamic height contours were only weakly varying.
339 Accordingly, there was no overall advantage of replacing latitude by dynamic height as a predictor of
340 biogenic mineral concentrations, and we have used latitude as the ordinate in our figures and
341 discussion.

342

343 Sea surface temperatures ($^{\circ}\text{C}$) were obtained from the NASA MODIS Aqua 11 μm night-only L3m
344 product available on-line:

345 [https://giovanni.gsfc.nasa.gov/giovanni/#service=TmAvMp&starttime=&endtime=&data=MODIS_](https://giovanni.gsfc.nasa.gov/giovanni/#service=TmAvMp&starttime=&endtime=&data=MODIS_L3m_SST_2014_nsst&variableFacets=dataFieldMeasurement%3ASea%20Surface%20Temperature%3B)
346 [L3m_SST_2014_nsst&variableFacets=dataFieldMeasurement%3ASea%20Surface%20Temperature](https://giovanni.gsfc.nasa.gov/giovanni/#service=TmAvMp&starttime=&endtime=&data=MODIS_L3m_SST_2014_nsst&variableFacets=dataFieldMeasurement%3ASea%20Surface%20Temperature%3B)
347 [%3B](https://giovanni.gsfc.nasa.gov/giovanni/#service=TmAvMp&starttime=&endtime=&data=MODIS_L3m_SST_2014_nsst&variableFacets=dataFieldMeasurement%3ASea%20Surface%20Temperature%3B)

348 We chose the night values to avoid shallow ephemeral structures arising from daytime solar heating.

349 We refer to these estimates simply as SST values.

350

351 Phytoplankton chlorophyll concentrations (Chl in $\text{mg m}^{-3} = \mu\text{g L}^{-1}$) were obtained from the NASA
352 MODIS Aqua L3m product available on-line:

353 [https://giovanni.gsfc.nasa.gov/giovanni/#service=TmAvMp&starttime=&endtime=&data=MODIS_](https://giovanni.gsfc.nasa.gov/giovanni/#service=TmAvMp&starttime=&endtime=&data=MODIS_L3m_CHL_2014_chlor_a&variableFacets=dataFieldMeasurement%3AChlorophyll%3B)
354 [L3m_CHL_2014_chlor_a&variableFacets=dataFieldMeasurement%3AChlorophyll%3B](https://giovanni.gsfc.nasa.gov/giovanni/#service=TmAvMp&starttime=&endtime=&data=MODIS_L3m_CHL_2014_chlor_a&variableFacets=dataFieldMeasurement%3AChlorophyll%3B)

355 The full citation for this data is:

356 NASA Goddard Space Flight Center, Ocean Ecology Laboratory, Ocean Biology Processing Group.

357 Moderate-resolution Imaging Spectroradiometer (MODIS) Aqua Chlorophyll Data; 2014

358 Reprocessing. NASA OB.DAAC, Greenbelt, MD, USA.

359 doi:10.5067/AQUA/MODIS/L3M/CHL/2014.

360 The algorithm relies on the blue/green reflectance ratio for Chl values above $0.2 \mu\text{g L}^{-1}$ and
361 incorporates stray light correction based on the difference between red and blue light reflectances at
362 lower Chl levels. This product has been suggested to underestimate chlorophyll in the Southern Ocean
363 south of Australia (Johnson et al., 2013), but has the advantage of ongoing ready availability. For this
364 reason, we use it only for context and not for any detailed comparisons to shipboard observations. We
365 refer to these estimates as SChl values.

366

367 Particulate inorganic carbonate concentrations (mol m^{-3}) based on backscatter magnitudes [*W M Balch*
368 *et al.*, 2005] were obtained from the NASA MODIS/AQUA ocean colour product available on-line:

369 https://oceancolor.gsfc.nasa.gov/cgi/l3/A20111212011151.L3m_MO_PIC_pic_9km.nc.png?sub=img

370 The full citation for this data is:

371 NASA Goddard Space Flight Center, Ocean Ecology Laboratory, Ocean Biology Processing Group.

372 Moderate-resolution Imaging Spectroradiometer (MODIS) Aqua Particulate Inorganic Carbon Data;



373 2014 Reprocessing. NASA OB.DAAC, Greenbelt, MD, USA. doi:

374 10.5067/AQUA/MODIS/L3M/PIC/2014.

375 We refer to these estimates as SPIC values. The veracity of these estimates in the Southern Ocean
376 remains an active area of research. PIC sampling in the Subantarctic South Atlantic found levels 2-3
377 times lower than the satellite estimates [W M Balch *et al.*, 2011], and the algorithm also produces
378 surprisingly high estimates in Antarctic waters, where limited shipboard surveys suggest that
379 coccolithophore abundances drop strongly (work summarized in Balch *et al.*, 2005). Our data
380 provides the most extensive PIC observations for comparison to SPIC values in Antarctic waters yet
381 available, and is discussed in detail below.

382

383 Modeled coccolithophore distributions were obtained from the data-assimilating general circulation
384 model NASA Ocean Biogeochemical Model (NOBM) available on-line:

385 https://giovanni.gsfc.nasa.gov/giovanni/#service=TmAvMp&starttime=&endtime=&data=NOBM_M
386 [ON_R2014_coc&variableFacets=dataFieldDiscipline%3AOcean%20Biology%3BdataFieldMeasure](https://giovanni.gsfc.nasa.gov/giovanni/#service=TmAvMp&starttime=&endtime=&data=NOBM_M)
387 [ment%3APhytoplankton%3B](https://giovanni.gsfc.nasa.gov/giovanni/#service=TmAvMp&starttime=&endtime=&data=NOBM_M)

388 The phytoplankton function type model is based on [Watson W Gregg and Casey, 2007a]. Details of
389 particular relevance to comparisons with our observations are discussed in section 3.4.

390

391 **3. Results and Discussion**

392

393 **3.1 Representativeness of oceanographic sampling**

394 As shown in Figure 1, sampling covered all Southern Ocean zones from sub-tropical waters in the
395 north to seasonally sea-ice covered waters in the south (covering SST ranging from -1 to 23 °C).
396 Almost all samples were representative of high-nutrient low-chlorophyll Southern Ocean waters,
397 indicative of iron limitation. Exceptions occurred near Tasmania, where moderate levels of SChl
398 were occasionally present, and over the Antarctic shelf where locally very high levels of SChl were
399 present. Individual maps for each voyage leg of SChl are provided in the Supplementary Material and
400 of satellite reflectance based estimates of PIC (SPIC) below, and reveal that higher values of SChl and
401 SPIC are often associated with mesoscale structures, especially in the Subantarctic and Polar Frontal
402 Zones. This means that mesoscale variability makes satellite versus shipboard comparisons difficult,
403 and this problem is exacerbated by frequent cloud cover. Both techniques characterize the very upper
404 water column, with ship samples from ~4m depth and the satellite ocean colour observations
405 reflecting the e-folding penetration depth of ~10-15 m [Grenier *et al.*, 2015; Morel and Maritorea,
406 2001].

407

408 It appears likely that our single-depth sampling can be considered as representative of upper water
409 column phytoplankton concentrations, because pigment samples and profiles of beam attenuation and



410 night-time fluorescence from some of these voyages as well as previous work show that biomass is
411 generally well mixed in the upper water column, and that when subsurface chlorophyll maxima are
412 present they primarily reflect increased chlorophyll levels rather than increased phytoplankton
413 abundances [Andrew R. Bowie *et al.*, 2011a; A.R. Bowie *et al.*, 2011b; Parslow *et al.*, 2001; Rintoul
414 and Trull, 2001; Shadwick *et al.*, 2015; Trull *et al.*, 2001b; S. W. Wright *et al.*, 1996; S.W. Wright and
415 van den Enden, 2000]. This perspective is also consistent with the limited information on the depth
416 distributions of coccolithophores in the Southern Ocean, which generally exhibit relatively uniform
417 and maximal values (especially for the most abundant species, *Emiliana huxleyi*) within the surface
418 mixed layer [Findlay and Giraudeau, 2000; Holligan *et al.*, 2010; Mohan *et al.*, 2008; Takahashi and
419 Okada, 2000]. There is some evidence that this conclusion can also be applied to the PIC50
420 foraminiferal fraction, in that the most abundant of these organisms tend to co-locate with
421 phytoplankton in the mixed layer in the Southern Ocean [Mortyn and Charles, 2003].

422

423

424 3.2 Latitudinal distributions of BSi, PIC, and POC

425 All the Voyage Legs exhibited similar latitudinal variations of the measured chemical components
426 (Figure 3). BSi, predominantly derived from diatoms, was clearly the dominant biogenic mineral in
427 the south in Antarctic waters. PIC01 concentrations, predominantly derived from coccolithophores,
428 were highest in northern Subantarctic waters, although even there BSi was often present at similar
429 levels. Interestingly, PIC50 concentrations, predominantly derived from foraminifera, often exhibited
430 maxima in the middle of the Southern Ocean at latitudes of 55-60 °S. The latitudinal variations in all
431 these biogenic mineral concentrations were quite strong, exceeding two orders of magnitude. In
432 contrast, variations in POC were 10-fold smaller, and often quite uniform across the central Southern
433 Ocean, with maxima sometimes in the far north near Tasmania and sometimes in the far south over
434 the Antarctic shelf (Figure 3). Variations in BSi, PIC, and POC concentrations among the voyages, at
435 a given latitude, were smaller than these north-south trends. It seems likely that these smaller
436 variations were partly seasonal, in that the earliest seasonal voyage leg (VL4 in September) had lower
437 concentrations of every component. But across the other voyages, ranging from mid-November
438 (VL5) to mid-April (VL1) no clear seasonal cycle was exhibited, perhaps owing to variations in
439 sampling location, and the known importance of inter-annual and mesoscale structures in Southern
440 Ocean phytoplankton distributions (e.g. [Moore *et al.*, 1999; Moore and Abbott, 2002; S. Sokolov and
441 Rintoul, 2007b]). As noted in the Methods section (2.3), the BSi values for VL1 stand out as being too
442 low, in that they were well below those of other voyages, while the POC, PIC01, and PIC50 values
443 were similar.

444

445 The latitudinal dependence of the relative importance of diatoms and coccolithophores is revealed by
446 viewing the BSi/PIC01 ratios as an ensemble for all the voyages (use of the ratio helps to remove



447 seasonal and interannual variations in their abundances which tend to track each other at a given
448 latitude). The BSi/PIC01 ratio reaches values of 200 in the far south and decreases north of 50 °S to
449 values near 1 (Figure 4a). Approximate equivalence of BSi and PIC01 occurs relatively far north in
450 the Southern Ocean, near 50 °S, and thus near the southern edge of the Subantarctic Zone. This
451 persistence of the importance of diatoms as a major component of the phytoplankton community in
452 northern waters of the Southern Ocean must reflect the winter-time renewal of silica supply from
453 upwelled deep waters in the Southern Ocean that are carried north by Ekman transport, combined
454 with recycling of biogenic silica within surface waters, given that by mid-summer silicate is largely
455 depleted north of the Subantarctic Front [Nelson *et al.*, 2001; Trull *et al.*, 2001b]. Accordingly the
456 relative dominance of diatoms and coccolithophores in the SAZ may be quite sensitive to changes in
457 the overturning circulation and westerly wind field. How this might translate into impacts on the
458 biological carbon pump remains far from clear. Interestingly, deep ocean sediment traps in the SAZ
459 south of Australia reveal strong dominance (4-fold) of PIC over BSi in the export flux to the ocean
460 interior, reminding us that export can be selective (and also that foraminifera can contribute a
461 significant fraction of total PIC, estimated to vary from ~1/3 to 2/3; [A L King and Howard, 2003]).
462 The POC flux recovered by these deep sediment traps was close to the global median and similar to
463 that of biogenic silica dominated fluxes in the Polar Frontal Zone to the south [Trull *et al.*, 2001a].
464

465 The importance of diatoms across the entire Southern Ocean, relative to coccolithophores is further
466 emphasized by expressing their biogenic mineral abundances in terms of associated POC, using
467 average values for the POC/BSi ratio of iron-limited diatoms (3.35, equivalent to a Si/N ratio of 2 and
468 Redfield C/N ratio of 6.7 [Ragueneau *et al.*, 2006; Takeda, 1998]) and the POC/PIC ratio of
469 coccolithophores (0.833, for *Emiliania huxleyi*, the dominant Southern Ocean species, [Bach *et al.*,
470 2015; M. N. Muller *et al.*, 2015]). As shown in Figure 4b, this suggests that diatoms dominate the
471 accumulation of organic carbon throughout the Southern Ocean, with coccolithophores generally
472 contributing less than half that of diatoms in the SAZ and less than a tenth of that in Antarctic waters.
473 Figure 4b also emphasizes that total POC contents can be largely explained by diatom abundances in
474 Antarctic waters (south of 50 °S), whereas in the SAZ (north of 50 °S), total POC often exceeds the
475 sum of contributions from diatoms and coccolithophores. This serves as an important reminder that
476 other organisms are important to the carbon cycle in the SAZ, and phytoplankton functional type
477 models should avoid over-emphasis on diatoms and coccolithophores just because they have
478 discernable biogeochemical impacts (on silica and alkalinity, respectively) and satellite remote
479 sensing signatures [Hood *et al.*, 2006; Moore *et al.*, 2002]. Finally, we note that the relatively low
480 abundance of pelagic calcifying organisms across the Southern Ocean as observed here means that
481 POC/PIC ratios are high, greater than 4 in the SAZ and ranging up to 20 in Antarctic waters (Figure
482 4a). This suggests calcification has a negligible countering impact on the reduction of CO₂ partial
483 pressure by phytoplankton uptake, and thus in mediating CO₂ transfer from the atmosphere into the



484 surface ocean, even smaller than the few to ~10% influence identified earlier from deep sediment trap
485 compositions in HNLC [*P. W. Boyd and Trull, 2007a*] and iron-enriched waters, respectively [*Salter*
486 *et al., 2014*].

487

488 Notably, our Southern Ocean PIC01 estimates are smaller than those found in northern hemisphere
489 polar waters. As compiled by Balch et al. (2005), concentrations were 100-fold higher (~10 μM) in
490 the north Atlantic south of Iceland (60-63 °N) than any of our values, and 1000-fold higher than our
491 values in the same southern hemisphere latitude range. Values collected over many years from the
492 Gulf of Maine [*W M Balch et al., 2008*] were ~ 1 μM , and thus 5-10 times higher than our SAZ
493 values (Gulf of Maine summer temperatures are similar to the SAZ, and colder in winter). This
494 difference between hemispheres is also evident in observations from the South Atlantic, where PIC
495 values estimated from acid labile backscatter for 6 voyages between 2004 and 2008 and latitudes 40-
496 50 °S were ~0.1-0.5 μM in remote waters [*W M Balch and Utgoff, 2009*], increasing to 1-2 μM in the
497 Argentine Basin with a few values reaching 4 μM [*W Balch et al., 2014*]. These high South Atlantic
498 observations are the highest of the “Great Calcite Belt” identified as a circumpolar feature of
499 Subantarctic waters based on SPIC values [*W Balch et al., 2014; W M Balch et al., 2011*]. Notably,
500 shipboard PIC measurements in this feature are 2-3 times lower than the SPIC estimates in the South
501 Atlantic [*W M Balch et al., 2011*], and ship collected samples from two voyages across the South
502 Atlantic and Indian sectors [*W M Balch et al., 2016*] exhibit PIC concentrations (actual PIC values
503 accessed online at <http://www.bco-dmo.org/dataset/560357>, rather than the PIC estimates from acid-
504 labile backscatter shown in the paper) that decrease eastwards in this feature to reach values close to
505 our observations in the Australian sector of ~ 0.1 μM (Figure 3).

506

507 **3.3 Comparison to satellite PIC (SPIC) estimates**

508 As is very evident from the limited observations we have achieved from our efforts over many years,
509 it will never be possible to characterize Southern Ocean phytoplankton population dynamics from
510 ship based sampling – the influences of mesoscale circulation, ephemeral inputs of the limiting
511 nutrient iron, and food web dynamics produce variability that cannot be adequately assessed in this
512 way, leaving sparse sampling open to potentially large biases. Use of satellite observations is clearly
513 the path forward to alleviate this problem, and development of algorithms for global coccolithophore
514 distributions has been a major advance [*W M Balch et al., 2005; Brown and Yoder, 1994*]. Until
515 recently the calibration of these SPIC values has been based primarily on North Atlantic observations.
516 Work to check these efforts for the Southern Ocean has begun, but remains sparse. Early work in the
517 South Atlantic found that SPIC values appeared to exceed in ocean PIC by a factor of 2-3 [*W M Balch*
518 *et al., 2011*], and based on a handful of samples it was suggested that this might reflect a lower
519 amount of PIC per coccolith [*Holligan et al., 2010*]. Two dedicated voyages to investigate the “Great



520 Calcite Belt” in the SAZ and PFZ across the South Atlantic and South Indian Oceans, attempted
521 comparison of acid-labile backscatter (as a proxy for PIC) and MODIS SPIC values, but there were no
522 match-ups in the South Atlantic owing to cloudy conditions [W M Balch *et al.*, 2016]. Results from
523 the South Indian sector, and from other voyages in the South Atlantic show high acid-labile
524 backscatter which translates into high SPIC estimates in the SAZ and PFZ (especially in naturally
525 iron-fertilized waters), but also high values further south which are not in agreement with ship
526 observations [W M Balch *et al.*, 2016; Smith *et al.*, 2017].

527

528 Comparison of our ship observations to MODIS SPIC estimates are shown in Figure 5 for each
529 voyage leg. These reveal some agreement in the SAZ in terms of identifying moderate levels of PIC,
530 often in association with higher levels of total SCHL (Supplementary Material), but differ strongly in
531 Antarctic waters where all ship observations reveal low PIC values, whereas the SPIC estimates in
532 Antarctic waters reach and often exceed those in the SAZ, especially over the Antarctic shelf. Our
533 sparse data do not permit a comparison in the SAZ sufficient to quantify possible differences between
534 the SPIC and PIC values there (only ~20 cloud-free match-ups were achieved, and about half of these
535 in waters with very low PIC), but are in rough agreement with the earlier estimate of an over-
536 estimation by the satellite algorithm of a factor of 2-3 [W M Balch *et al.*, 2011].

537

538 **3.4 Comparison to possible environmental controls on coccolithophore growth rates**

539 The ship observations provided here offer a significant advance in quantifying the distributions of
540 coccolithophores in the Southern Ocean south of Australia, but much less understanding of why these
541 distributions arise and therefore how they might change in response to climate, circulation, and
542 biogeochemical changes in the future. Coccolithophores, especially the most common species
543 *Emiliana huxleyi*, have been studied sufficiently in the laboratory to allow possible important
544 controls on their niches and especially their calcification rates to be proposed, including temperature,
545 pH, pCO₂, calcite saturation state, and macro- and micro-nutrient availability [Bach *et al.*, 2015; Feng
546 *et al.*, 2016; Mackinder *et al.*, 2010; M. N. Muller *et al.*, 2015; M.N. Muller *et al.*, 2017; Schlüter *et al.*,
547 *et al.*, 2014; Schulz *et al.*, 2007; Sett *et al.*, 2014]. We collected observations of many of these properties
548 in parallel with our PIC observations, and now briefly examine whether they present correlations that
549 might contribute to understanding why coccolithophores are found mainly in northern Subantarctic
550 waters, and not further south. For illustrative purposes, we focus on VL3 (the mid- to late summer 19
551 northward hydrographic section from Antarctica to Perth) and VL6 (the early to mid-summer
552 southward Astrolabe transit from Tasmania to Antarctica). VL3 covered the widest range of physical
553 properties, and exhibited PIC01 concentrations that remained elevated further south than any other
554 voyage (Figure 3). VL6 exhibited the more typical PIC01 distribution of a close to continuous
555 decrease southward (Figure 3). The results from the other Voyage Legs were very similar to VL3
556 (figures not shown; data available in Supplementary Materials)..



557

558 Many properties that might influence coccolithophore productivity decreased strongly and close to
559 monotonically from north to south across the Southern Ocean for our voyages (Figure 6). These
560 include temperature (from 23 to -0.4 C for our samples), salinity (from 35.6 to 33.6, with tight
561 correlation with alkalinity, not shown - data available in the Supplementary Material), pH (from 8.20
562 to 8.08 on the free scale), and the saturation state of calcite (from 5.22 to 2.12). The strong
563 correlation of these properties means that it is not easy to separate their possible influences on
564 coccolithophore distributions, without relying on specific thresholds or quantitative response models.
565 With the added complexity of a lack of information on individual species, or the availability of iron as
566 the limiting micro-nutrient, deducing a possible influence of ocean acidification on coccolithophore
567 distributions from our spatial distribution data is very difficult, and well beyond our scope.
568 Nonetheless, we offer a few pertinent observations. Firstly, the change in PIC01 abundances with
569 latitude is much larger than expected from models of the responses of calcification rates (normalized
570 to maximum rates) to inorganic carbon system variations (Figure 6). Two models are shown:

571

572 The “Bach model” based on independent terms for sensitivity to bicarbonate, CO₂, and pH. It fits
573 quite well the results from many laboratory incubations of *Emiliana Huxleyi* strains under conditions
574 of modern and elevated pCO₂ [Bach *et al.*, 2015], and we have used values for the constants (a, b, c,
575 d) obtained from incubations of a strain isolated from Subantarctic waters south of Tasmania [Miller
576 *et al.*, 2017] to provide what might be considered the best current model for the calcification rate
577 response to changing inorganic carbon abundance and speciation, following Eq. (1):

578

$$579 \quad \text{Bach relative calcification rate} = a [\text{HCO}_3^-] / (b + [\text{HCO}_3^-]) - e^{-c[\text{CO}_2]} - d[\text{H}^+] \quad (1)$$

580

581 The “Langdon model” based on a simple, inorganic precipitation motivated parameterization of
582 calcification as a function of calcite saturation state Ω [Gattuso *et al.*, 1998; Langdon *et al.*, 2000],
583 which has been shown to apply in an approximate way to many corals [Anthony *et al.*, 2011;
584 Silverman *et al.*, 2007], and perhaps to Southern Ocean foraminifera [Moy *et al.*, 2009]. We have
585 chosen the simple linear form (n=1) and a sensitivity at the top end of the observed range (a = 1/4, so
586 that calcification rate varies linearly from 0 to 1 for $\Omega=1$ to 4), following Eq. (2):

587

$$588 \quad \text{Langdon relative calcification rate} = a (\Omega - 1)^n \quad (2)$$

589

590

591 As shown in Figure 6, both these calcification rate models exhibit limited variations with latitude in
592 the Southern Ocean. The Bach model suggests negligible change in calcification rate. This is



593 essentially because the Southern Ocean variations in bicarbonate, CO₂, and pH are very small
594 compared to the future expected values used in incubation experiments. In addition, southward
595 cooling causes pH to rise, offsetting the impact of southward decrease in salinity and alkalinity, thus
596 reducing the southward decrease of pH and the associated drop in modeled calcification rate. The
597 Langdon model suggests approximately 3-fold decrease in calcification rate, which is considerably
598 smaller than the more than 10-fold drop in PIC01 (shown on a linear scale in Figure 6 and a
599 logarithmic scale in Figure 3). The shape of the Langdon model decrease shows some agreement with
600 that of PIC01 for VL6, but none for VL3 (which exhibits relatively constant significant PIC01
601 concentrations in the 40-50 °S latitude range where the Langdon model shows a strong decrease in
602 calcification rate, and then a strong drop in PIC01 south of 60 °S where the Langdon model shows no
603 change). Thus, and unsurprisingly, coccolithophore abundances are clearly not controlled by
604 inorganic carbon chemistry alone.

605

606 Many laboratory studies have emphasized the importance of temperature on coccolithophore growth
607 rates, as compiled recently [Feng *et al.*, 2016], and warming has been suggested as a possible cause of
608 decadal northward apparent range expansion in the North Atlantic [Rivero-Calle *et al.*, 2015] and the
609 occurrence of unusual blooms in the Bering Sea [Merico *et al.*, 2004]. To provide a brief
610 visualization of the expected univariate response, we fit the “Norberg” thermal optimum envelope
611 model [Norberg, 2004] to growth rate data for 5-25 °C with modern pCO₂ and nutrient replete
612 conditions for a Southern Ocean morphotype A strain of *Emiliana Huxleyi*, isolated from south of
613 Tasmania [M. N. Muller *et al.*, 2015], with optimum temperature $z=15$, thermal window $w=10$, and
614 scaling constant a , in which the exponential term represents the broad global temperature dependence
615 of generic phytoplankton growth rates [Eppley, 1972] and produces the known skewed form of
616 organismic thermal tolerances, following Eq. (3):

617

$$618 \quad \text{Norberg growth rate (d}^{-1}\text{)} = a [1 - ((T-z)/w)^2] e^{0.0633T} \quad (3)$$

619

620 As shown in Figure 6, this predicts a drop from ~0.5 d⁻¹ at the northern edge of the Southern Ocean to
621 zero growth near ~53 °S, whereas PIC01 concentrations fall off more slowly further south. The
622 presence of other morphotypes with lower thermal optima [Cubillos *et al.*, 2007] is an easy possible
623 way to explain this difference. Overall the Norberg temperature model has an advantage of the
624 calcification rate models – it does predict a strong decrease to negligible PIC01 values in the south.
625 There are of course many other possible explanations.

626

627 Interestingly, these uncertainties regarding the roles of inorganic carbon chemistry and temperature on
628 Southern Ocean coccolithophore distributions contrast with the possible role of macro-nutrients, in
629 that phosphate and nitrate increase southward across the Southern Ocean (e.g. [Trull *et al.*, 2001b]),



630 and were everywhere abundant during our surveys (nitrate > 3 μM , with phosphate/nitrate close to
631 Redfield expectations, data in Supplementary Material), and thus would be expected to lead to
632 southward increases in coccolithophore abundances which were not observed. For this reason we
633 suggest nitrate and phosphate availability is not an obvious driver of the southward decrease in
634 coccolithophore abundances in Southern Ocean HNLC waters (i.e. these nutrients are sufficient
635 everywhere), although these nutrients may be important in determining the success of
636 coccolithophores in oligotrophic waters at the northern edge of the Southern ocean, given the high
637 half-saturation constant for nitrate uptake observed in some laboratory studies ($\sim 13 \mu\text{M}$; [Feng *et al.*,
638 2016]), and the possibility that high temperature and low nutrient conditions may non-linearly amplify
639 phytoplankton stresses [Thomas *et al.*, 2017].

640
641 Importantly, in addition to multivariate environmental control of coccolithophore distributions via
642 their growth rates, there is the possibility of control by resource competition with other autotrophs
643 (presumably mainly for iron) and/or stronger loss terms to grazers in Antarctic than Subantarctic
644 waters. These are difficult issues to evaluate, and we provide just one comment. Diatom abundances
645 as estimated from BSi concentrations show a stronger latitudinal relationship to silicon availability
646 than coccolithophores do to carbonate availability (Figure 6). Diatoms abundances drop strongly near
647 the SAF, north of which summer time $\text{Si}(\text{OH})_4$ concentrations drop below 1 μM , i.e. close to the
648 ‘residual’ concentration which it appears diatoms cannot access [Paasche, 1973]. Surveys of
649 coccolithophores and diatoms in the SAZ in the South Atlantic and South Indian sectors have
650 previously suggested that coccolithophore distributions may be linked to competition with diatoms [W
651 M Balch *et al.*, 2016; Smith *et al.*, 2017], and this view is compatible with our observations, although
652 it remains unproven. Further progress in understanding the controls on coccolithophore abundances in
653 the Southern Ocean is clearly needed. At present temperature and competition with diatoms for iron
654 appear to be the strongest candidates (at least for southward expansion; with nitrate a strong influence
655 on the location of the northern oligotrophic boundary; [Feng *et al.*, 2016]).

656

657 3.5 Comparison to the NASA Ocean Biogeochemical Model

658 Many of these ideas about the roles of environmental conditions and ecological competition have
659 been included in models for global coccolithophore distributions, e.g. [Watson W Gregg and Casey,
660 2007a; Le Quere *et al.*, 2005]; and we provide a brief comparison to one model – the NASA Ocean
661 Biogeochemical Model (NOBM) for which simulation results are available on-line (see the Methods
662 section). In brief, the NOBM predicts coccolithophore abundances (in Chl units) that are restricted to
663 the far northern reaches of the Southern Ocean (Figure 7). This is also true for the Dynamic Green
664 Ocean Model [Le Quere *et al.*, 2005]. This contrasts with our PIC results (Figures 3, 4, 6) and with
665 PIC and coccolithophore cell counts from other sampling efforts which have found coccolithophore
666 abundances to extend with similar concentrations right across the SAZ and sometimes the PFZ, e.g.



667 during VL6 south of western Australia (Figures 3 and 6), south of Tasmania [*Cubillos et al.*, 2007],
668 in the Scotia Sea [*Holligan et al.*, 2010], and in the South Atlantic and South Indian Oceans,
669 especially in regions of natural iron fertilization [*W M Balch et al.*, 2016; *Smith et al.*, 2017]. In the
670 NOBM, diatoms are also simulated and show (Figure 7) the expected high abundance in Antarctic
671 waters in the southern third of the Southern Ocean, decreasing northward as in our results (but also
672 show a band of elevated diatom concentrations in the Subantarctic, which we did not observe).

673
674 Competition for nutrients in the NOBM favours the ability of coccolithophores over diatoms to get by
675 on limited resources (half-saturation constants for nitrate and iron of 0.5 and 0.67 versus 1.0 and 1.0
676 μM) including light (half saturation constant of 56 versus 90 $\mu\text{mol photons m}^{-2} \text{s}^{-1}$ under Southern
677 Ocean low light conditions). But diatoms are specified to have higher growth rates when all resources
678 are non-limiting (maximum growth rate at 20 °C 1.50 versus 1.13, both with the same Eppley
679 dependence on temperature). Thus in the model, diatoms dominate silicon replete Southern Ocean
680 waters, outcompeting other species for the limiting iron, and only give way to other species when
681 silicon is depleted. Notably these other species then do best when additional Fe is supplied from
682 either atmospheric sources (in the north where continental dusts are not shielded by ice) or island
683 oases such as Crozet or Kerguelen. This view is compatible with our observations and those carried
684 out in the northern half of the Southern Ocean during the “Great Calcite Belt” voyages [*W M Balch et*
685 *al.*, 2016; *Smith et al.*, 2017]. It suggests that potential expansion of coccolithophores southward
686 might be linked to decreasing supply of silicon from reduced upwelling of Circumpolar Deep Water
687 in a progressively more stratified global ocean. A cautionary note to this conclusion is provided by
688 the NOBM simulation of significant concentrations of diatoms in the SAZ where silicon is low, which
689 arises from their specified higher maximum growth rate, emphasizing the importance of this
690 parameter, and its temperature dependence, in modeling phytoplankton distributions. In specifying
691 this temperature dependence, this model and most others still rely on the global compilation from
692 nearly 50 years ago [*Eppley*, 1972]. Clearly better understanding of the controls on maximum growth
693 rates and their temperature tolerance for key phytoplankton taxa is needed, first to understand current
694 distributions and then to explore possible future changes.

695

696

697

698

699

700

701 4. Conclusions

702 Our surveys of PIC concentrations as a proxy for coccolithophores in the Southern Ocean south of
703 Australia suggest:



704

705

- The concentrations of coccolithophores were much smaller (at least 10-fold) in the open Southern Ocean south of Australia than in northern hemisphere oceans.

706

707

708

- Coccolithophores were most abundant in the Subantarctic Zone, and occasionally in the Polar Frontal Zone.

709

710

711

- The contribution of coccolithophores to total phytoplankton biomass (estimated from POC)

712

was small, less than 10% in Subantarctic waters and less than 1% in Antarctic waters.

713

714

- The “Great Calcite Belt” characterization of SAZ and PFZ waters based on satellite estimates of PIC (SPIC) is overstated south of Australia. The SPIC estimates appear to be too high by a factor of 2-3 in the SAZ, and given their low contribution to total PIC it does not appear that coccolithophores have a dominant role regional marine ecology.

715

716

717

- Even greater care must be taken in the use of satellite PIC (SPIC) estimates south of the Subantarctic Front, because the algorithms erroneously identify large agglomerations of PIC where none is present south of Australia.

718

719

720

- Our PIC results and ancillary measurements of biogenic silica, particulate organic carbon, dissolved nutrients, and inorganic carbon system status may be useful in the testing of models of limiting conditions and ecological competitions that affect coccolithophore distributions. Preliminary considerations suggest that temperature, iron, and competition with diatoms may be stronger influences than pH or calcite saturation state.

721

722

723

724

725

726

727

728

729

730

731

Despite the considerable effort required to obtain these survey results, much remains to be done just to define coccolithophore distributions, for example their seasonality, especially when the complexities of differing responses of individual species and strains are considered.

732

733

734

735

736

737



738 ***Acknowledgements***

739 We thank Steve Rintoul (CSIRO Oceans and Atmosphere, Hobart) and Alain Poisson (Universite
740 Pierre et Marie Curie, Paris) for allowing sample collection to proceed under the auspices of their
741 science programs onboard *Aurora Australis* and *l'Astrolabe*, respectively. ACE CRC staff, students,
742 and volunteers carried out onboard sampling, including Peter Jansen, Stephane Thannassekos,
743 Elizabeth Shadwick, and Nick Roden. Nutrient analyses were carried out by the CSIRO
744 hydrochemistry group. Thomas Rodemann at the UTAS Central Sciences Laboratory did the CHN
745 analyses. Funding was provided by the Australian Commonwealth Cooperative Research Centre
746 Program via the ACE CRC. Tim Smit participated in the first voyage in 2008 and described those
747 results in his Utrecht University Masters thesis and in a poster presented at the Second Symposium on
748 the Ocean in a High CO₂ World, Monaco, October 6-9, 2008. Andrew Lenton (CSIRO) produced the
749 database of absolute mean dynamic heights and associated front locations.

750

751

752 **References**

753

754 Anthony, K., J. A Kleypas, and J. P. Gattuso (2011), Coral reefs modify their seawater
755 carbon chemistry—implications for impacts of ocean acidification, *Global Change Biology*,
756 17(12), 3655-3666.

757 Bach, L. T., U. Riebesell, M. Gutowska, L. Federwisch, and K. G. Schulz (2015), A unifying
758 concept of coccolithophore sensitivity to changing carbonate chemistry embedded in an
759 ecological framework, *Progress in Oceanography*, 135, 125-138.

760 Balch, W., D. Drapeau, B. Bowler, E. Lyczkowski, L. Lubelczyk, S. Painter, and A. Poulton
761 (2014), Surface biological, chemical, and optical properties of the Patagonian Shelf
762 coccolithophore bloom, the brightest waters of the Great Calcite Belt, *Limnol. Oceanogr*,
763 59(5), 1715-1732.

764 Balch, W. M., N. R. Bates, P. J. Lam, B. S. Twining, S. Z. Rosengard, B. C. Bowler, D. T.
765 Drapeau, R. Garley, L. C. Lubelczyk, and C. Mitchell (2016), Factors regulating the Great
766 Calcite Belt in the Southern Ocean and its biogeochemical significance, *Global*
767 *Biogeochemical Cycles*, 30(8), 1124-1144.

768 Balch, W. M., D. T. Drapeau, B. C. Bowler, E. S. Booth, L. A. Windecker, and A. Ashe
769 (2008), Space–time variability of carbon standing stocks and fixation rates in the Gulf of
770 Maine, along the GNATS transect between Portland, ME, USA, and Yarmouth, Nova
771 Scotia, Canada, *Journal of plankton research*, 30(2), 119-139.

772 Balch, W. M., D. T. Drapeau, B. C. Bowler, E. Lyczkowski, E. S. Booth, and D. Alley
773 (2011), The contribution of coccolithophores to the optical and inorganic carbon budgets
774 during the Southern Ocean Gas Exchange Experiment: New evidence in support of the
775 "Great Calcite Belt" hypothesis, *Journal of Geophysical Research*, 116, C00F06,
776 doi:10.1029/2011JC006941.

777 Balch, W. M., H. R. Gordon, B. C. Bowler, D. T. Drapeau, and E. S. Booth (2005), Calcium
778 carbonate measurements in the surface global ocean based on Moderate-Resolution
779 Imaging Spectroradiometer data, *Journal of Geophysical Research*, 110, C07001; doi:
780 10.1029/2004jc002560.

781 Balch, W. M., and P. E. Utgoff (2009), Potential interactions among ocean acidification,
782 coccolithophores, and the optical properties of seawater, *Oceanography*, 22(4), 146-159.

783 Be, A. W. H., and D. Tolderlund (1971), Distribution and ecology of living planktonic
784 foraminifera in surface waters of the Atlantic and Indian Oceans, in *Micropaleontology of*



- 785 *Oceans* edited by B. M. Funnel and W. R. Riedel, pp. 105-149, Cambridge University
786 Press, New York.
- 787 Boeckel, B., K.-H. Baumann, R. Henrich, and H. Kinkel (2006), Coccolith distribution
788 patterns in South Atlantic and Southern Ocean surface sediments in relation to
789 environmental gradients, *Deep Sea Research Part I: Oceanographic Research Papers*,
790 53(6), 1073-1099, doi:<http://dx.doi.org/10.1016/j.dsr.2005.11.006>.
- 791 Bowie, A. R., F. B. Griffiths, F. Dehairs, and T. W. Trull (2011a), Oceanography of the
792 subantarctic and Polar Frontal Zones south of Australia during summer: Setting for the
793 SAZ-Sense study, *Deep-Sea Research II*, 58(21-22), 2059-2070,
794 doi:10.1016/j.dsr2.2011.05.033.
- 795 Bowie, A. R., T. W. Trull, and F. Dehairs (2011b), Estimating the Sensitivity of the
796 Subantarctic Zone to Environmental Change: the SAZ-Sense project., *Deep Sea Research*
797 *II*, 58(21-22), 2051-2058.
- 798 Boyd, P. W., and T. Trull (2007a), Understanding the export of biogenic particles in oceanic
799 waters: Is there consensus?, *Progress in Oceanography*, 72(4), 276-312,
800 doi:10.1016/j.pocean.2006.10.007.
- 801 Boyd, P. W., and T. W. Trull (2007b), Understanding the export of marine biogenic particles:
802 is there consensus?, *Progress in Oceanography*, 4, 276-312,
803 doi:10.1016/j.pocean.2006.10.1007.
- 804 Brown, C. W., and J. A. Yoder (1994), Coccolithophore blooms in the global ocean., *Journal*
805 *of Geophysical Research*, 104C, 1541-1558.
- 806 Buitenhuis, E., P. van der Wal, and H. J. W. de Baar (2001), Blooms of *Emiliania huxleyi* are
807 sinks of atmospheric carbon dioxide: a field and mesocosm study derived simulation,
808 *Global Biogeochemical Cycles*, 15(3), 577-587.
- 809 Cao, L., and K. Caldeira (2008), Atmospheric CO₂ stabilization and ocean acidification,
810 *Geophysical Research Letters*, 35(19), n/a-n/a, doi:10.1029/2008GL035072.
- 811 Cubillos, J. C., S. W. Wright, G. Nash, M. F. d. Salas, B. Griffiths, B. Tilbrook, A. Poisson,
812 and G. M. Hallegraeff (2007), Calcification morphotypes of the coccolithophorid
813 *Emiliania huxleyi* in the Southern Ocean: changes in 2001 to 2006 compared to historical
814 data, *Marine Ecology Progress Series*, 348, 47-54, doi: 10.3354/meps07058.
- 815 Dickson, A. G., C. L. Sabine, and J. R. Christian (2007), Guide to Best Practices for Ocean
816 CO₂ Measurements, *Report*, North Pacific Marine Sciences Association, Sidney, British
817 Columbia, http://cdiac.ornl.gov/oceans/Handbook_2007.html



- 818 Doubleday, A. J., and R. R. Hopper (2015), Interannual patterns during spring and late
819 summer of larvaceans and pteropods in the coastal Gulf of Alaska, and their relationship to
820 pink salmon survival, *Journal of Plankton Research*, 37(1), 134-150,
821 doi:10.1093/plankt/fbu092.
- 822 Eppley, R. W. (1972), Temperature and phytoplankton growth in the sea, *Fisheries Bulletin*,
823 70, 1063-1085.
- 824 Eriksen, R. (1997), A practical manual for the determination of salinity, dissolved oxygen,
825 and nutrients in seawater, Antarctic Cooperative Research Centre *Report 11*, 83 pp,
826 Hobart, Tasmania, Australia.
- 827 Eynaud, F., J. Giraudeau, J. J. Pichon, and C. J. Pudsey (1999), Sea-surface distribution of
828 coccolithophores, diatoms, silicoflagellates and dinoflagellates in the South Atlantic
829 Ocean during the late austral summer 1995, *Deep Sea Research Part I: Oceanographic
830 Research Papers*, 46(3), 451-482, doi:[http://dx.doi.org/10.1016/S0967-0637\(98\)00079-X](http://dx.doi.org/10.1016/S0967-0637(98)00079-X).
- 831 Feng, Y., M. Y. Roleda, E. Armstrong, P. W. Boyd, and C. L. Hurd (2016), Environmental
832 controls on the growth, photosynthetic and calcification rates of a Southern Hemisphere
833 strain of the coccolithophore *Emiliania huxleyi*, *Limnology and Oceanography*, 62, 519-
834 540, doi:10.1002/lno.10442.
- 835 Findlay, C. S., and J. Giraudeau (2000), Extant calcareous nannoplankton in the Australian
836 Sector of the Southern Ocean (austral summers 1994 and 1995), *Marine
837 Micropaleontology*, 40(4), 417-439, doi:[http://dx.doi.org/10.1016/S0377-8398\(00\)00046-](http://dx.doi.org/10.1016/S0377-8398(00)00046-3)
838 3.
- 839 Gattuso, J.-P., M. Frankignoulle, I. Bourge, S. Romaine, and R. Buddemeier (1998), Effect of
840 calcium carbonate saturation of seawater on coral calcification, *Global and Planetary
841 Change*, 18(1), 37-46.
- 842 Gravalosa, J. M., J.-A. Flores, F. J. Sierro, and R. Gersonde (2008), Sea surface distribution
843 of coccolithophores in the eastern Pacific sector of the Southern Ocean (Bellingshausen
844 and Amundsen Seas) during the late austral summer of 2001, *Marine Micropaleontology*,
845 69(1), 16-25, doi:<http://dx.doi.org/10.1016/j.marmicro.2007.11.006>.
- 846 Gregg, W. W., and N. W. Casey (2007b), Modeling coccolithophores in the global oceans,
847 *Deep Sea Research Part II: Topical Studies in Oceanography*, 54(5-7), 447-477,
848 doi:<http://dx.doi.org/10.1016/j.dsr2.2006.12.007>.
- 849 Grenier, M., A. Della Penna, and T. W. Trull (2015), Autonomous profiling float
850 observations of the high biomass plume downstream of the Kerguelen plateau in the
851 Southern Ocean, *Biogeosciences* 12, 1-29, doi:10.5194/bg-12-1-2015.



- 852 Holligan, P., A. Charalampopoulou, and R. Hutson (2010), Seasonal distributions of the
853 coccolithophore, *Emiliania huxleyi*, and of particulate inorganic carbon in surface waters
854 of the Scotia Sea, *Journal of Marine Systems*, 82(4), 195-205.
- 855 Hood, R. R., E. A. Laws, R. A. Armstrong, N. R. Bates, C. W. Brown, C. A. Carlson, F.
856 Chai, S. C. Doney, P. G. Falkowski, and R. A. Feely (2006), Pelagic functional group
857 modeling: Progress, challenges and prospects, *Deep Sea Research Part II: Topical Studies*
858 *in Oceanography*, 53(5), 459-512.
- 859 Kimball Jr, J., and E. Ferguson Wood (1964), A simple centrifuge for phytoplankton studies,
860 *Bulletin of Marine Science*, 14(4), 539-544.
- 861 King, A. L., and W. R. Howard (2003), Planktonic foraminiferal flux seasonality in
862 Subantarctic sediment traps: A test for paleoclimate reconstructions, *Paleoceanography*,
863 18(1), 1019, doi:10.1029/2002PA000839, 002003.
- 864 King, P., H. Kennedy, P. P. Newton, T. D. Jickells, T. Brand, S. Calvert, G. Cauwet, H.
865 Etcheber, B. Head, and A. Khripounoff (1998), Analysis of total and organic carbon and
866 total nitrogen in settling oceanic particles and a marine sediment: an interlaboratory
867 comparison, *Marine Chemistry*, 60(3), 203-216.
- 868 Klaas, C., and D. E. Archer (2002), Association of sinking organic matter with various types
869 of mineral ballast in the deep sea: Implications for the rain ratio, *Global Biogeochemical*
870 *Cycles*, 16(4), doi:10.1029/2001GB001765.
- 871 Langdon, C., T. Takahashi, C. Sweeney, D. W. Chipman, and J. Goddard (2000), Effect of
872 calcium carbonate saturation state on the calcification rate on an experimental coral reef,
873 *Global Biogeochemical Cycles*, 14(2), 613C-DIC, 615N-NO613 and 618O-NO613 639-
874 654.
- 875 Le Quere, C., S. P. Harrison, I. Colin Prentice, E. T. Buitenhuis, O. Aumont, L. Bopp, H.
876 Claustre, L. Cotrim Da Cunha, R. Geider, and X. Giraud (2005), Ecosystem dynamics
877 based on plankton functional types for global ocean biogeochemistry models, *Global*
878 *Change Biology*, 11(11), 2016-2040.
- 879 Mackinder, L., G. Wheeler, D. Schroeder, U. Riebesell, and C. Brownlee (2010), Molecular
880 mechanisms underlying calcification in coccolithophores, *Geomicrobiology Journal*,
881 27(6), 585-595.
- 882 McNeil, B. I., and R. J. Matear (2008), Southern Ocean acidification: A tipping point at 450-
883 ppm atmospheric CO₂, *Proceedings of the National Academy of Sciences* 105(48), 18860-
884 18864, doi: 18810.11073/pnas.0806318105.



- 885 Merico, A., T. Tyrrell, E. J. Lessard, T. Oguz, P. J. Stabeno, S. I. Zeeman, and T. E.
886 Whittedge (2004), Modelling phytoplankton succession on the Bering Sea shelf: role of
887 climate influences and trophic interactions in generating *Emiliana huxleyi* blooms 1997–
888 2000, *Deep Sea Research I*, 51(12), 1803-1826, doi:1810.1016/j.dsr.2004.1807.1003.
- 889 Mohan, R., L. P. Mergulhao, M. V. S. Guptha, A. Rajakumar, M. Thamban, N. AnilKumar,
890 M. Sudhakar, and R. Ravindra (2008), Ecology of coccolithophores in the Indian sector of
891 the Southern Ocean, *Marine Micropaleontology*, 67(1–2), 30-45,
892 doi:<http://dx.doi.org/10.1016/j.marmicro.2007.08.005>.
- 893 Moore, J. K., M. R. Abbot, J. G. Richman, W. O. Smith, T. J. Cowles, K. H. Coale, G. W.D.,
894 and R. T. Barber (1999), SeaWiFS satellite ocean color data from the Southern Ocean,
895 *Geophysical Research Letters*, 26(10), 1465-1468.
- 896 Moore, J. K., and M. R. Abbott (2002), Surface chlorophyll concentrations in relation to the
897 Antarctic Polar Front: seasonal and spatial patterns from satellite observations, *Journal of*
898 *Marine Systems*, 37, 69-86.
- 899 Moore, J. K., S. C. Doney, J. A. Kleypas, D. M. Glover, and I. Y. Fung (2002), An
900 intermediate complexity marine ecosystem model for the global domain, *Deep-Sea*
901 *Research II*, 49, 403-462?
- 902 Morel, A., and S. Maritorena (2001), Bio-optical properties of oceanic waters- A reappraisal,
903 *Journal of Geophysical research*, 106(C4), 7163-7180.
- 904 Mortyn, P. G., and C. D. Charles (2003), Planktonic foraminiferal depth habitat and $\delta 18O$
905 calibrations: Plankton tow results from the Atlantic sector of the Southern Ocean,
906 *Paleoceanography*, 18(2).
- 907 Moy, A. D., W. Howard, S. G. Bray, and T. Trull (2009), Reduced calcification in modern
908 Southern Ocean planktonic foraminifera, *Nature Geoscience*, 2(April), 276-280,
909 doi:10.1038/NGEO460.
- 910 Muller, M. N., T. Trull, and G. M. Hallegraeff (2015), Differing responses of three Southern
911 Ocean *Emiliana huxleyi* ecotypes to changing seawater carbonate chemistry, *Marine*
912 *Ecology Progress Series*, 531, 81-90, doi:10.3354/meps11309.
- 913 Müller, M. N., T. W. Trull, and G. M. Hallegraeff (2017), Independence of nutrient limitation
914 and carbon dioxide impacts on the Southern Ocean coccolithophore *Emiliana huxleyi*,
915 *The ISME Journal*, 1-11, doi:10.1038/ismej.2017.53.
- 916 Nelson, D. M., M. A. Brzezinski, D. E. Sigmon, and V. M. Frank (2001), A seasonal
917 progression of Si limitation in the Pacific sector of the Southern Ocean, *Deep-Sea*
918 *Research II*, 48, 3973-3995.



- 919 Norberg, J. (2004), Biodiversity and ecosystem functioning: a complex adaptive systems
920 approach, *Limnology and Oceanography*, 49(4part2), 1269-1277.
- 921 Olbers, D. J., V. Gouretski, and G. S. J. Schroter (1992), *Hydrographic Atlas of the Southern*
922 *Ocean*, 99 pp., Alfred Wegener Institute for Polar and Marine Research, Bremerhaven.
- 923 Orr, J. C., et al. (2005), Anthropogenic ocean acidification over the twenty-first century and
924 its impact on calcifying organisms, *Nature* 437, 681-686, doi:610.1038/nature04095.
- 925 Paasche, E. (1973), Silicon and the ecology of marine plankton diatoms. I. *Thalassiosira*
926 *pseudonana* (*Cyclotella nana*) grown in a chemostat with silicate as limiting nutrient,
927 *Marine biology*, 19(2), 117-126.
- 928 Parslow, J., P. Boyd, S. R. Rintoul, and F. B. Griffiths (2001), A persistent sub-surface
929 chlorophyll maximum in the Polar Frontal Zone south of Australia: seasonal progression
930 and implications for phytoplankton-light-nutrient interactions, *Journal of Geophysical*
931 *Research*, 106, 31543-31557.
- 932 Pörtner, H. O., M. Langenbuch, and B. Michaelidis (2005), Synergistic effects of temperature
933 extremes, hypoxia, and increases in CO₂ on marine animals: From Earth history to global
934 change, *Journal of Geophysical Research, Oceans*, 110, doi:10.1029/2004JC002561.
- 935 Pujol, M.-I., Y. Faugère, G. Taburet, S. Dupuy, C. Pelloquin, M. Ablain, and N. Picot (2016),
936 DUACS DT2014: the new multi-mission altimeter data set reprocessed over 20 years,
937 *Ocean Science*, 12(5), 1067-1090.
- 938 Ragueneau, O., S. Schultes, K. Bidle, P. Claquin, and B. Moriceau (2006), Si and C
939 interactions in the world ocean: Importance of ecological processes and implications for
940 the role of diatoms in the biological pump, *Global Biogeochemical Cycles*, 20(4),
941 GB4S02.
- 942 Ridgwell, A., D. N. Schmidt, C. Turley, C. Brownlee, M. T. Maldonado, P. Tortell, and J. R.
943 Young (2009), From laboratory manipulations to Earth system models: scaling
944 calcification impacts of ocean acidification, *Biogeosciences*, 6, 2611-2623.
- 945 Rintoul, S. R., and T. Trull (2001), Seasonal evolution of the mixed layer in the Subantarctic
946 Zone south of Australia, *Journal of Geophysical Research*, 106(C12), 31447-31462,
947 doi:10.1029/2000JC000329.
- 948 Rivero-Calle, S., A. Gnanadesikan, C. E. Del Castillo, W. M. Balch, and S. D. Guikema
949 (2015), Multidecadal increase in North Atlantic coccolithophores and the potential role of
950 rising CO₂, *Science*, 350(6267), 1533-1537.
- 951 Roberts, D., W. R. Howard, J. L. Roberts, S. G. Bray, A. D. Moy, T. Trull, and R. R.
952 Hopcroft (2014), Diverse trends in shell weight of three Southern Ocean pteropod taxa



- 953 collected with Polar Frontal Zone sediment traps from 1997 to 2007, *Polar Biology*,
954 37(10), 1445-1458, doi:10.1007/s00300-014-1534-6.
- 955 Roden, N. P., B. Tilbrook, T. W. Trull, P. Virtue, and G. D. Williams (2016), Carbon cycling
956 dynamics in the seasonal sea-ice zone of East Antarctica, *Journal of Geophysical*
957 *Research: Oceans*, doi:10.1002/2016JC012008.
- 958 Rost, B., and U. Riebesell (2004), Coccolithophores and the biological pump: responses to
959 environmental changes, in *Coccolithophores*, edited, pp. 99-125, Springer.
- 960 Salter, I., R. Schiebel, P. Ziveri, A. Movellan, R. Lampitt, and G. A. Wolff (2014), Carbonate
961 counter pump stimulated by natural iron fertilization in the Polar Frontal Zone, *Nature*
962 *Geosci*, 7(12), 885-889, doi:10.1038/ngeo2285.
- 963 Schiebel, R. (2002), Planktic foraminiferal sedimentation and the marine calcite budget,
964 *Global Biogeochemical Cycles*, 16(4), 1065.
- 965 Schlüter, L., K. T. Lohbeck, M. A. Gutowska, J. P. Gröger, U. Riebesell, and T. B. Reusch
966 (2014), Adaptation of a globally important coccolithophore to ocean warming and
967 acidification, *Nature Climate Change*, 4(11), 1024-1030.
- 968 Schulz, K. G., B. Rost, S. Burkhardt, U. Riebesell, S. Thoms, and D. Wolf-Gladrow (2007),
969 The effect of iron availability on the regulation of inorganic carbon acquisition in the
970 coccolithophore *Emiliania huxleyi* and the significance of cellular compartmentation for
971 stable carbon isotope fractionation, *Geochimica et Cosmochimica Acta*, 71(22), 5301-
972 5312.
- 973 Sett, S., L. T. Bach, K. G. Schulz, S. Koch-Klavsen, M. Lebrato, and U. Riebesell (2014),
974 Temperature modulates coccolithophorid sensitivity of growth, photosynthesis and
975 calcification to increasing seawater pCO₂, *PLoS One*, 9(2), e88308.
- 976 Shadwick, E. H., B. Tilbrook, N. Cassar, T. W. Trull, and S. R. Rintoul (2015), Summertime
977 physical and biological controls on O₂ and CO₂ in the Australian Sector of the Southern
978 Ocean, *Journal of Marine Systems*, 147, 21-28, doi:10.1016/j.jmarsys.2013.12.008.
- 979 Shadwick, E. H., T. Trull, H. Thomas, and J. A. E. Gibson (2013), Vulnerability of Polar
980 Oceans to Anthropogenic Acidification: Comparison of Arctic and Antarctic Seasonal
981 Cycles, *Scientific Reports*, 3(August), 1-7, doi:10.1038/srep02339.
- 982 Silverman, J., B. Lazar, and J. Erez (2007), Effect of aragonite saturation, temperature, and
983 nutrients on the community calcification rate of a coral reef, *Journal of Geophysical*
984 *Research: Oceans*, 112(C5).
- 985 Smith, H. E., A. J. Poulton, R. Garley, J. Hopkins, L. C. Lubelczyk, D. T. Drapeau, S.
986 Rauschenberg, B. S. Twining, N. R. Bates, and W. M. Balch (2017), The influence of



- 987 environmental variability on the biogeography of coccolithophores and diatoms in the
988 Great Calcite Belt, *Biogeoscience Discussions, in review*, doi:10.5194/bg-2017-5110.
- 989 Sokolov, S., and S. R. Rintoul (2002), Structure of Southern Ocean fronts at 140E, *Journal of*
990 *Marine Systems*, 37(1-3), 151-184.
- 991 Sokolov, S., and S. R. Rintoul (2007a), Multiple jets of the Antarctic Circumpolar Current
992 south of Australia, *Journal of Physical Oceanography*, 37, 1394-1412,
993 doi:1310.1175/JPO3111.1391.
- 994 Sokolov, S., and S. R. Rintoul (2007b), On the relationship between fronts of the Antarctic
995 Circumpolar Current and surface chlorophyll concentrations in the Southern Ocean, *J.*
996 *Geophys. Res. – Oceans*, 112(C07030), doi: 10.1029/2006JC004072.
- 997 Takahashi, K., and H. Okada (2000), Environmental control on the biogeography of modern
998 coccolithophores in the southeastern Indian Ocean offshore of Western Australia, *Marine*
999 *Micropaleontology*, 39(1-4), 73-86, doi:http://dx.doi.org/10.1016/S0377-8398(00)00015-
1000 3.
- 1001 Takeda, S. (1998), Influence of iron availability on nutrient consumption ratio of diatoms in
1002 oceanic waters, *Nature*, 393, 774-777.
- 1003 Thomas, M. K., M. Aranguren-Gassis, C. T. Kremer, M. R. Gould, K. Anderson, C. A.
1004 Klausmeier, and E. Litchman (2017), Temperature–nutrient interactions exacerbate
1005 sensitivity to warming in phytoplankton, *Global Change Biology*, doi:10.1111/gcb.13641.
- 1006 Trull, T., S. G. Bray, S. J. Manganini, S. Honjo, and R. Francois (2001a), Moored sediment
1007 trap measurements of carbon export in the Subantarctic and Polar Frontal Zones of the
1008 Southern Ocean, south of Australia, *Journal of Geophysical Research*, 106(C12), 31489-
1009 31509, doi:10.1029/2000JC000308.
- 1010 Trull, T., S. R. Rintoul, M. Hadfield, and E. R. Abraham (2001b), Circulation and seasonal
1011 evolution of polar waters south of Australia: Implications for iron fertilization of the
1012 Southern Ocean, *Deep-Sea Research Part II-Topical Studies in Oceanography*, 48(11-12),
1013 2439-2466, doi:10.1016/s0967-0645(01)00003-0.
- 1014 Van Heuven, S., D. Pierrot, J. Rae, E. Lewis, and D. Wallace (2011), MATLAB program
1015 developed for CO₂ system calculations, ORNL/CDIAC-105b, Carbon Dioxide Inf. *Anal.*
1016 *Cent., Oak Ridge Natl. Lab., US DOE, Oak Ridge, Tenn.*
- 1017 Wright, S. W., D. P. Thomas, H. J. Marchant, H. W. Higgins, M. D. Mackey, and D. J.
1018 Mackey (1996), Analysis of phytoplankton of the Australian sector of the Southern Ocean:
1019 comparisons of microscopy and size frequency data with interpretations of pigment HPLC



1020 data using the 'CHEMTAX' matrix factorisation program, *Marine Ecology Progress*
1021 *Series, 144*, 285-298.
1022 Wright, S. W., and R. L. van den Enden (2000), Phytoplankton community structure and
1023 stocks in the East Antarctic marginal ice zone (BROKE survey, Jan.-Mar.1996)
1024 determined by CHEMTAX analysis of HPLC pigment signatures, *Deep-Sea Research II*,
1025 *47*(12), 2363-2400.
1026
1027



1028 **Figure Captions**

1029 1. Map of sample sites (dots) relative to major Southern Ocean fronts (lines) and satellite SST (means
1030 for productive months, October-March, over the sample collection period 2008-2014).

1031

1032 2. Comparison of centrifugation versus filtration size-fraction results for Voyage Leg 1, a)
1033 centrifugation total POC versus filtration POC (0.8-50 μm fraction): b) centrifugation total PIC
1034 versus filtration PIC01 (0.8-50 μm) and PIC50 (50-1000 μm) fractions.

1035

1036 3. Latitudinal variations in POC, BSi, PIC50, PIC01 concentrations for each voyage leg. See Table 1
1037 for Voyage Leg details and Figure 1 for sample sites.

1038

1039 4. Latitudinal variations in the dominance of diatoms versus coccolithophores and their contributions
1040 to total POC, for results combined from all voyages: a) BSi/PIC01 and POC/(PIC50+PIC01) ratios, b)
1041 Percent contributions to total POC attributable to diatoms (assuming POC/BSi=3.35) and
1042 coccolithophores (assuming POC/PIC01=0.833).

1043

1044 5. Maps comparing ship based distributions of coccolithophore PIC distributions (PIC01, coloured
1045 dots) with satellite PIC estimates (SPIC; background colours) for each voyage leg. The SPIC
1046 estimates are averages for the month preceding the start of each voyage leg. Contour lines indicate
1047 dynamic height determined frontal positions for the week preceding the each voyage leg (see Figure 1
1048 for front nomenclature).

1049

1050 6. Latitudinal environmental conditions for voyage leg VL3 (left panels) and voyage leg VL6 (right
1051 panels): a, b) T, S, pH (free scale), calcite saturation, c, d) PIC01, Bach and Langdon relative
1052 calcification rate (dimensionless) and Norberg growth rate (d^{-1}) models, e, f) BSi and $\text{Si}(\text{OH})_4$
1053 concentrations (μM).

1054

1055 7. Maps of NASA Ocean Biogeochemical Model results for coccolithophore and diatom distributions
1056 Results are means for productive month, October-March for 2008-2012, the last year available on-
1057 line: a) diatoms, b) coccolithophores.

1058

1059

**Table 1. Sample Collection**

#	Voyage Name	Leg	Dates	PIC50 ³	PIC01	POC	BSi
VL1	AA2008_V6 (SR3)	North	28/03/08–15/04/08	57/0	59/0	59/0	59/0
VL2	AA2012_V3 (I9)	South	05/01/12–20/01/12 ¹	4/16	4/16	9/25	7/22
VL3	AA2012_V3 (I9)	North	20/01/12–09/02/12	62/0	62/0	59/0	53/0
VL4	AA2012_VMS (SIPEXII)	South	13/09/12–22/09/12	0/21	0/20	0/24	0/24
VL5	AA2012_VMS (SIPEXII)	North	11/11/12–15/11/12	0/25	0/25	0/27	0/28
VL6	AL2013_R2 (Astrolabe)	South	10/01/13–15/01/13	0/25	0/25	0/23	0/25
VL7	AL2013_R2 (Astrolabe)	North	25/01/13–30/01/13	0/27	0/27	0/26	0/27
VL8	AA2014_V2 (Totten)	South	05/12/14–11/12/14	0/36	0/36	0/32	0/37
VL9	AA2014_V2 (Totten)	North	22/12/14–24/01/15 ²	6/44	6/44	8/27	8/39

¹ 18/01/12–20/01/12 east-west traverse from ~ 65° S 144° E to 65° S 113° E included in South leg

² 22/12/14–11/1/15 west-east traverse from ~ 65° S 110° E to 65° S 140° E included in North leg

³ Numbers of samples collected on station / underway

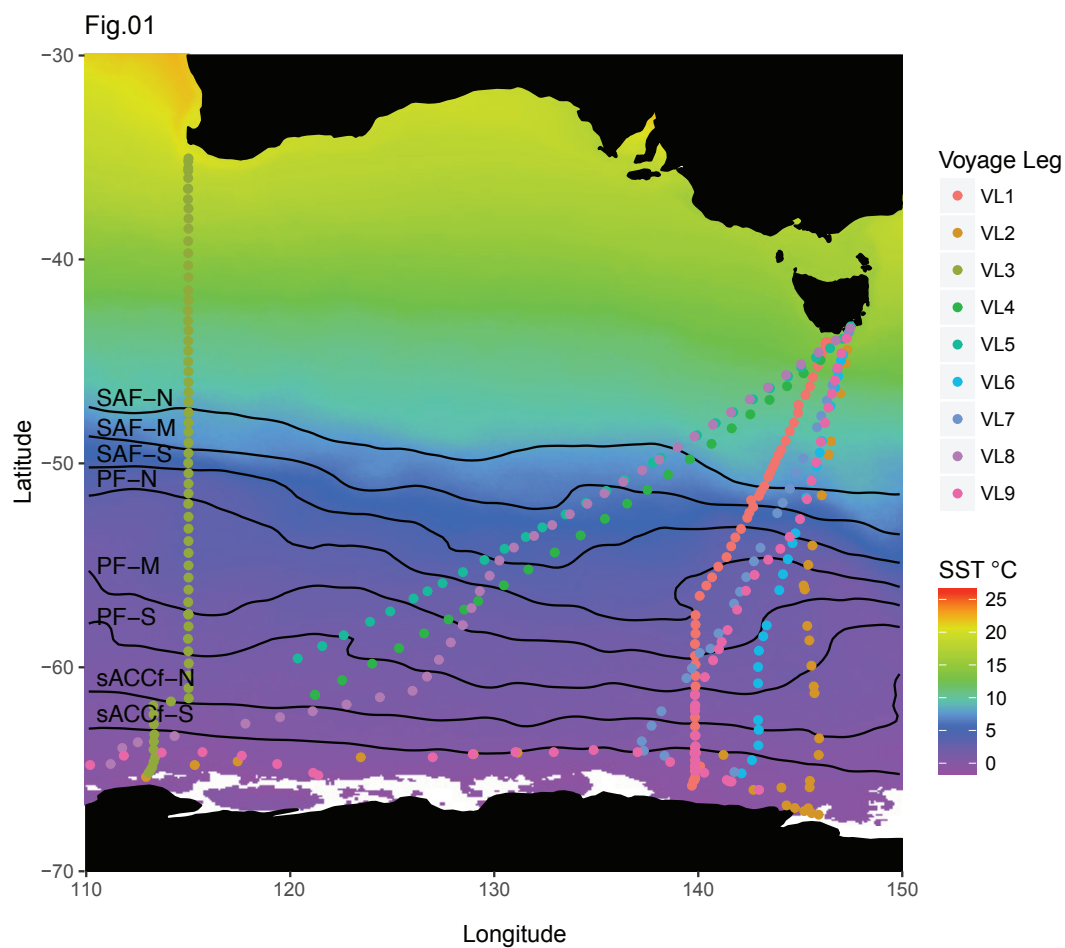




Fig.2

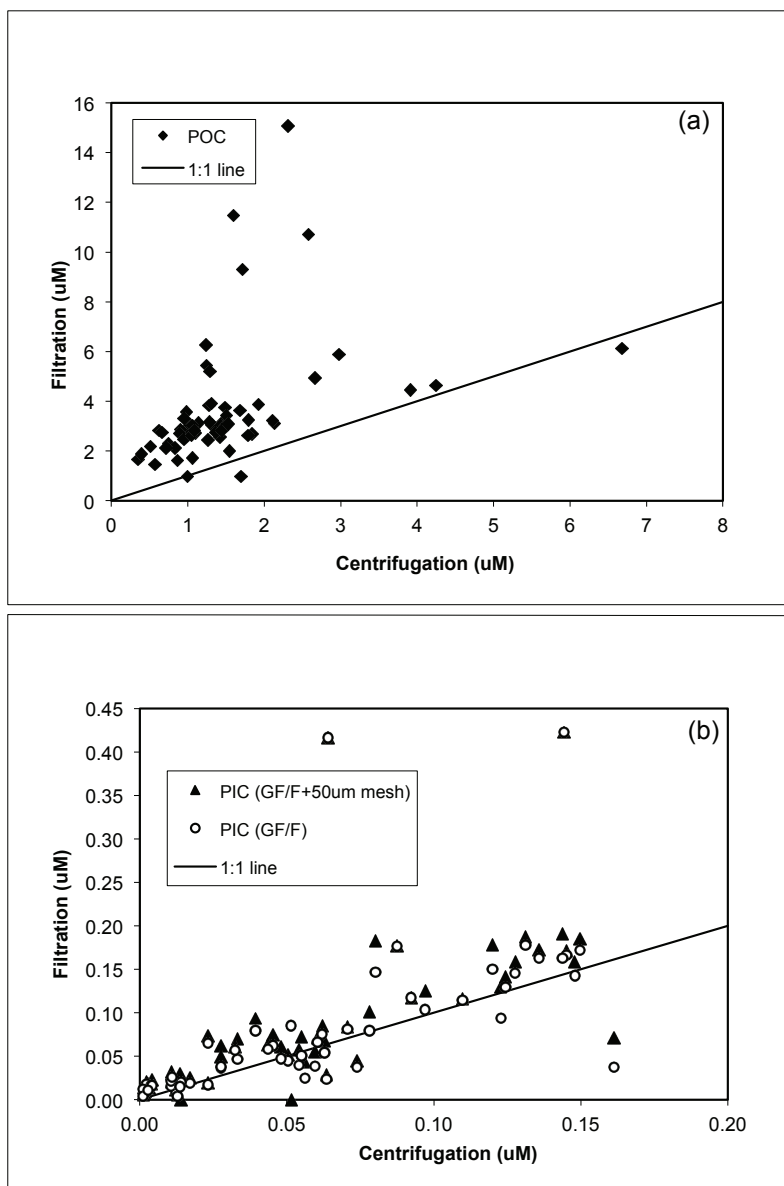




Fig.03

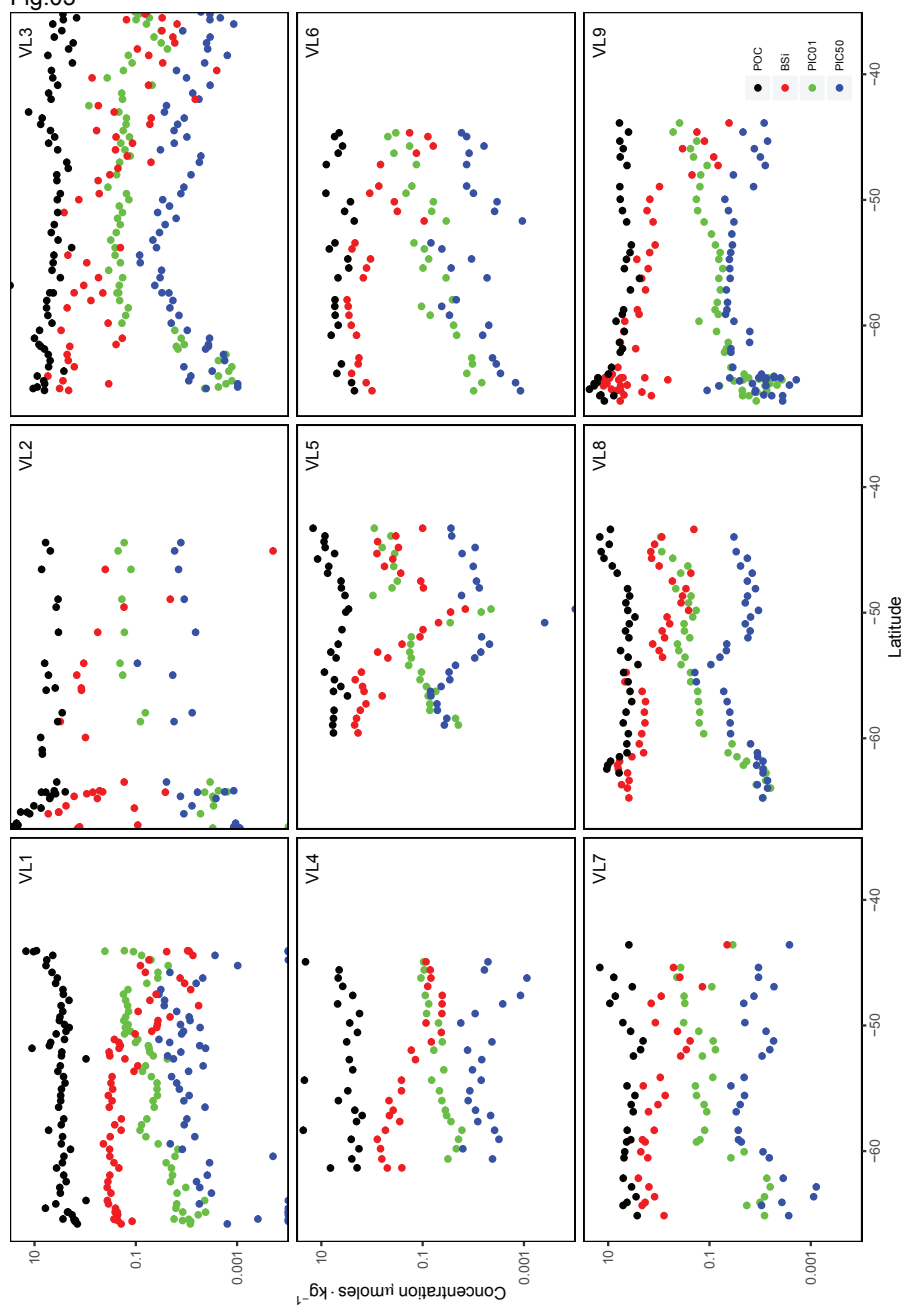




Fig.04

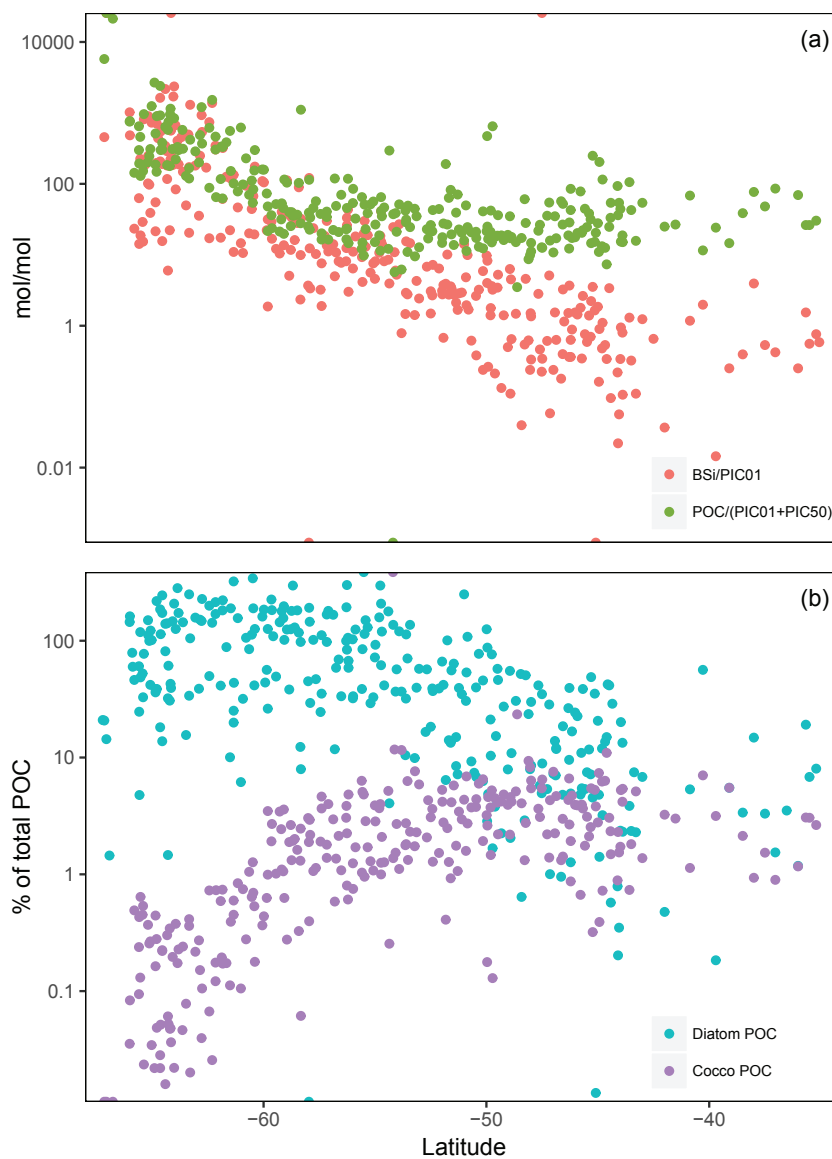




Fig.05

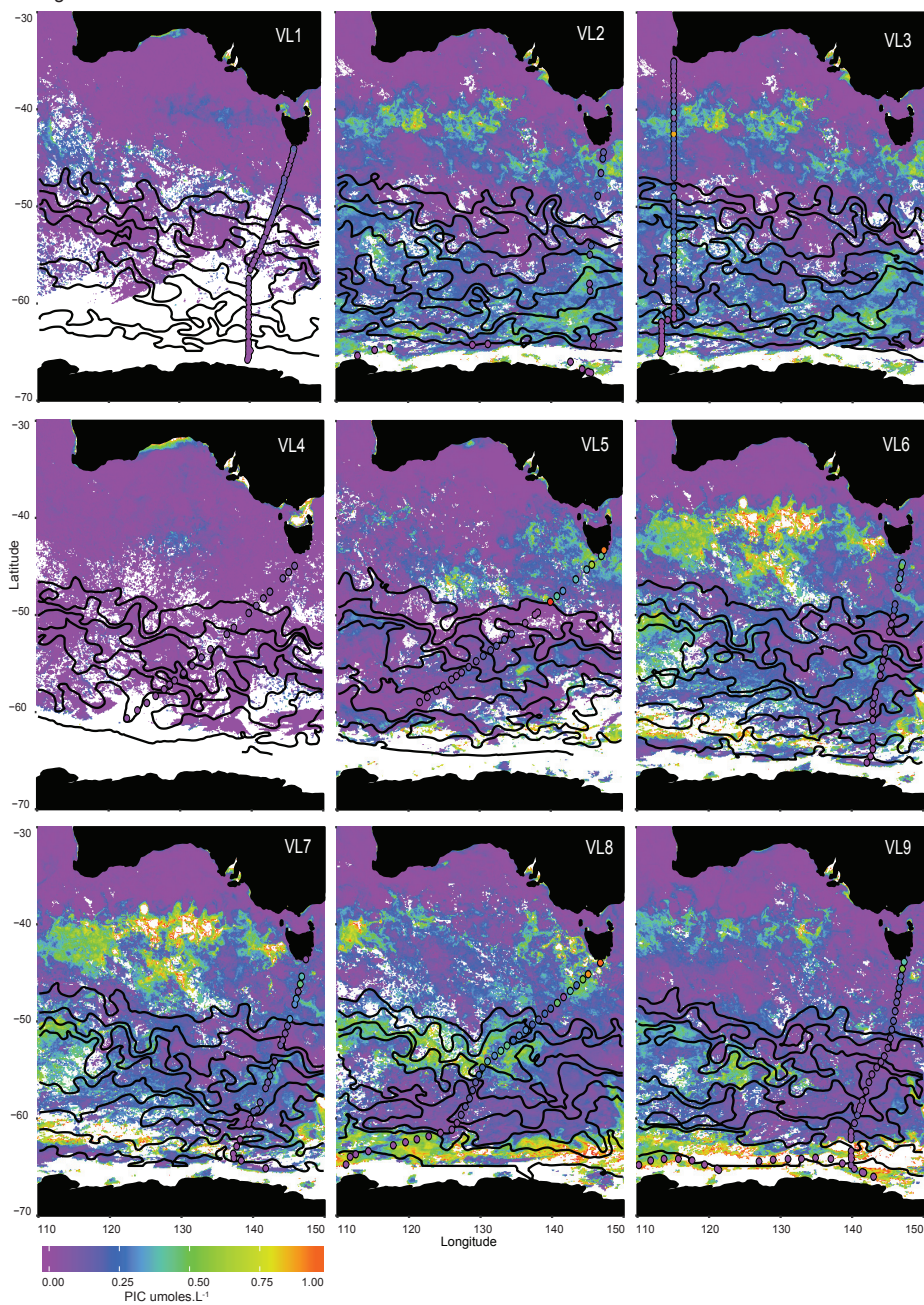




Fig.06

